Geological Quarterly, 2025, 69, 7
DOI: http://dx.doi.org/10.7306/gq.1780

Taxonomic position of the brown bear *Ursus arctos* remains from Niedźwiedzia Cave (Silesia, SW Poland) and the problem of extreme species morphological variability

Adrian MARCISZAK[1, *] and Wiktoria GORNIG[2]

[1] University of Wrocław, Department of Palaeozoology, Sienkiewicza 21, 50–335 Wrocław, Poland; ORCID: 0000-0002-1472-6553

[2] University of Wrocław, Department of Evolutionary Biology and Conservation of Vertebrates, Sienkiewicza 21, 50–335 Wrocław, Poland; ORCID: 0000-0001-9273-2409

Marciszak, A., Gornig, W., 2025. Taxonomic position of the brown bear *Ursus arctos* remains from Niedźwiedzia Cave (Silesia, SW Poland) and the problem of extreme species morphological variability. Geological Quarterly, 69, 7; https://doi.org/10.7306/gq.1780

Associate editor: Michał Zatoń

Abundant and well preserved fossil material from Niedźwiedzia Cave documents the presence of two different subspecies of *Ursus arctos*: the Late Pleistocene *Ursus arctos taubachensis* and the Holocene *Ursus arctos arctos*. Apart from a few bones of the Holocene age, the vast majority of the material is dated to MIS 3 and represents large individuals of robust posture, typical of the cold phases of the Late Pleistocene. *Ursus arctos taubachensis* is a characteristic element of Late Pleistocene steppe-tundra faunas and was a highly carnivorous scavenger. Our analysis shows that some individuals from Niedźwiedzia Cave are among the largest ever found. Revision of the characters distinguishing these two subspecies of *Ursus arctos* shows the equal importance of metrical and morphological features. Apart the larger size and wider teeth, the main feature is the more robust build of *Ursus arctos taubachensis*, especially of the metapodials. For the highly mobile *Ursus arctos*, DNA is shown to be less important in the determination of subspecies when dealing with the material from the Central European sites.

Key words: taxonomy; ecomorph, teeth, metapodials, size decreasing.

INTRODUCTION

Ursus arctos Linnaeus, 1758 is a Holarctic species distributed across different environmental and climatic conditions encompassing boreal, montane, arctic, forest and open habitats. Across this broad range, this bear exhibits enormous variability in ecology, genetics, behaviour and morphology (Erdbrink, 1953; Baryshnikov, 2007; Haroldson et al., 2020; Swenson et al., 2020). *U. arctos* is well adapted to cold environments with dense fur, large fat stores, adaptability to various food sources, and the ability to reduce energy expenditure during winter by decreasing metabolism because of hibernation. The survival skills of this species are among the highest in all extant carnivores. This gives it great adaptability, an enormous ecological tolerance and the capability to occupy different habitats. Due to such a broad distribution, *U. arctos* is highly polymorphic. Therefore, it has been split into a number of subspecies based on phenotypic differences (Erdbrink, 1953; Baryshnikov, 2007). A similar patttern has been obtained in studies of fossil materials. Because of the impossibility of collecting genetic information on older bones, morphological analyses are often the only approach that can be used to study the evolutionary lineage of the brown bear. However, this normally entails difficulties in defining and estimating intra- and interspecific variability, both chronologically and geographically. Studies have shown the continual occurrence of *U. arctos* in Europe, even during the coldest periods of the Late Pleistocene (Sommer and Benecke, 2005; Valdiosera et al., 2008; Davison et al., 2011; Edwards et al., 2014; Ersmark, 2016; Ersmark et al., 2019; Marciszak et al., 2019). There were no sufficient natural barriers for brown bear dispersion, and its continuous gene flow across most of the European territory was observed during that time (Ersmark et al., 2019; Kosintsev et al., 2019).

During these studies palaeontologists encountered remains of an arctoid bear which was metrically and morphologically distinct from the extant European brown bear. Those bears have been classified under multiple names: *U. ferox*, *horribilis*, *anglicus*, *priscus*, *arctoideus* etc. (Erdbrink, 1953). Their comparability in size with, and morphological similarity to, large cave bears led to suggestions of possible hybridisation between

* Corresponding author, e-mail: adrian.marciszak@uwr.edu.pl

Received: January 23, 2025; accepted: March 10, 2025; first published online: May 12, 2025

them (Ehrenberg, 1938). Recently, some of those remains have been revisited and re-described (Pacher, 2007; Baryshnikov, 2007; Marciszak et al., 2019, 2020, 2022, 2024a). Issues of significant ecological plasticity, enormous intraspecific variability and wide geographical range mean that the taxonomic position of *Ursus arctos priscus* is still not resolved. Since its first description (Goldfuss, 1818a, b), there are still no clearly defined morphological features to describe the steppe brown bear as a distinct form (Pacher, 2007; Baryshnikov, 2007; Marciszak et al., 2019, 2020, 2022, 2024a). The overwhelming majority of authors stated its great size as a key feature (Baryshnikov, 2007; Pacher, 2007; Marciszak et al., 2015, 2019).

In this study, we analysed the morphometric and morphological diversity of the fossil material of the brown bear from Niedźwiedzia Cave where, at one locality, two different forms have been found. Comparison with some genetic and isotopic data in the broader, Eurasian context offers a possibility to clarify this situation. However, questions still remain concerning the palaeogenetic and palaeoecological diversity of large Late Pleistocene bears and their relationships to the extant bears. Because the issue of size has been broadly discussed in the papers cited above, we here focus attention on morphological and metrical values.

MATERIAL AND METHODS

The material of *U. arctos* from Niedźwiedzia Cave has never previously been studied and described in detail (Appendix 1). All of the fossil material is stored in the Department of Palaeozoology, University of Wrocław. The fossils analysed in this paper were identified using basic morphometric analysis. Measurements were taken point to point with the Landmark system to the nearest 0.01 mm. Measurement schemas and teeth terminology are shown in Figures S1–S2 of Appendix 2. Measurements were taken using an Olympus set for image analysis (*Olympus stereomicroscope ZSX 12, camera Olympus DP 71, program Cell D*). A *Canon EOS 5D* camera was used to photograph the fossil material. Throughout the text, upper teeth are referred to by capital letters (e.g. P4) and lower teeth by lowercase letters (e.g. p4). The geological timescale and subdivisions are based on the International Chronostratigraphic Chart (v2024/12), approved by the International Commission on Stratigraphy (http://www.stratigraphy.org/index.php/ics-chart-timescale). For this purpose we also used the global chronostratigraphical correlation table for the last 2.7 million years, version 2022a (https://quaternary.stratigraphy.org/files/charts/POSTERstratchart_v2022a.pdf). Abbreviations used in the text are as follows: B – breadth, B ta – talonid m1 breadth, B tr – trigonid m1 breadth, JN – Niedźwiedzia Cave, L – length, L ta – talonid m1 length, L tr – trigonid m1 length, Ma – million years ago.

The most useful elements within the postcranial skeleton for biostratigraphic and taxonomic analyses are the metapodials, calcanei and talii. These are characterised by their abundant occurrence, solid structure and usually good and often complete state of preservation and morphology that allows for the selection of easily recognisable and clearly defined measurement points. Additionally, the observed metric changes significantly correlate with evolutionary changes over time. The methodology of using metapodials is according to Withalm (2001), with two basic coefficients:

1. T-index (TI), the shaft mass coefficient, calculated as the quotient of the smallest shaft width divided by the total length and multiplied by 100, i.e.
   TI = mB/L 100,
2. P-index (PI), the mass coefficient, calculated as the quotient of the width of the distal epiphysis measured above the condyles divided by the total length and multiplied by 100, i.e.
   PI = dB/L 100.

GEOLOGICAL SETTINGS

Niedźwiedzia Cave (55°68'70"N 36°31'65"E, 807–800 m a.s.l.) is located in the Sudety Mts, Silesia region, SW Poland (Fig. 1). Since its discovery in 14.10.1966 during marble exploitation, exploration of this cave has continued until the present. Its corridors are wholly or partly filled by allochthonous and autochthonous deposits such as rock debris, collapsed chamber scree deposits, fluvial gravels, sands, silts and dripstones (Sobczyk et al., 2016). The discovered length of the cave corridors exceeds 5000 m. Nevertheless, the total length of the cave corridors is much longer, as indicated by new results from geophysical imaging (Marciszak et al., 2024b). The cave was formed within marbles dated as Middle Cambrian to Early Ordovician (520–470 Ma). Their karstification began after the Paleogene basin inversion climax (65–45 Ma) before its final post-Mid-Miocene uplift. In Kleśnica Valley the karstification process, aligned with WSW–ENE trending sub-vertical faults and fractures, with N–S to NNW–SSE steeply dipping foliation, played a subordinate role. The cave morphology exhibits distinct structural patterns in two main different sections. The northern areas demonstrate a grid-like structure, while the southern regions feature elongated N–S passages (Fig. 1). The earliest passages, presumed to predate the Mid-Pleistocene, witnessed multiple phases of heightened tectonic activity and potential palaeoearthquakes(Marciszak et al., 2024b).

Intensive palaeontological investigations have been carried out mostly in the middle level of the locality, leading to the excavation of two faunal assemblages of different ages. The older one, dated back to MIS 3–2, includes *Sorex araneus* Linnaeus, 1758, *Crocidura suaveolens* (Pallas, 1811), *Castor fiber* Linnaeus, 1758, *Arvicola terrestris* (Linnaeus, 1758), *Microtus arvalis* (Pallas, 1779), *Microtus nivalis* (Martins, 1842), *Microtus agrestis* (Linnaeus, 1758), *Lepus europaeus* Pallas, 1778, *Canis lupus spelaeus* Goldfuss, 1823, *Vulpes vulpes* (Linnaeus, 1758), *Vulpes lagopus* (Linnaeus, 1758), *Ursus spelaeus ingressus* (Rabeder and Hofreiter, 2004), *Ursus arctos taubachensis*, *Gulo gulo* (Linnaeus, 1758), *Meles meles* (Linnaeus, 1758), *Martes martes* (Linnaeus, 1758), *Mustela erminea* Linnaeus, 1758, *Mustela nivalis* Linnaeus, 1758, *Panthera spelaea spelaea* (Goldfuss, 1810), *Cervus elaphus* Linnaeus, 1758, *Rangifer tarandus* (Linnaeus, 1758), *Bison priscus* (Bojanus, 1827), *Rupicapra rupicapra* (Linnaeus, 1758) and *Sus scrofa* Linnaeus, 1758. The remains of *U. s. ingressus* comprised around 98.5% of the findings (Marciszak et al., 2024b).

The composition of the younger faunal assemblage, dated to MIS 1, consists of *Talpa europaea* Linnaeus, 1758, *Sorex araneus*, *Eptesicus nilssoni* (Key et Blasius, 1839), *Myotis brandti* (Eversmann, 1845), *Myotis daubentoni* (Kuhl, 1819), *Myotis myotis* (Borkhausen, 1797), *Myotis mystacinus* (Kuhl, 1819), *Myotis nattereri* (Kuhl, 1818), *Myotis bechsteini* (Kuhl,

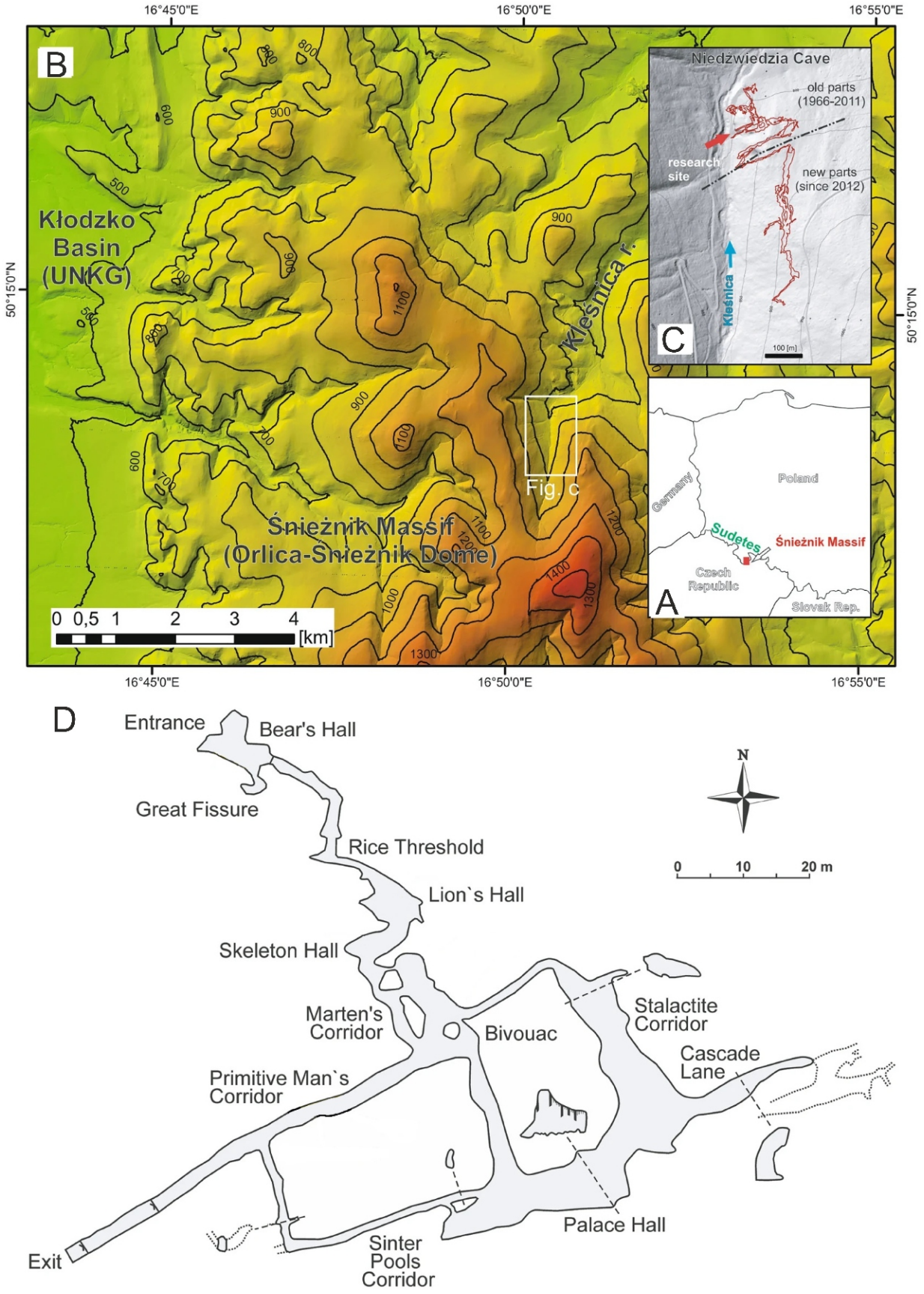

Fig. 1. Geographical location of Niedźwiedzia Cave in the Kleśnica River valley, in the Śnieżnik Massif in Poland, modified from Marciszak et al. (2024b: fig. 1)

A – the cave's position in Poland; **B** – details of the Śnieżnik Massif region with a white outline indicating the cave; **C** – representation of the 1966–2011 (upper) and post-2012 (lower) cave explorations; **D** – a cave plan showing the fossil-bearing areas (AI-AVI, KCP) and three silt profiles (JN-1, JN-2, JN-3) sampled for geochemical analyses

1818), *Plecotus auritus* (Linnaeus, 1758), *Lepus europaeus*, *Castor fiber*, *Sciurus vulgaris* Linnaeus, 1758, *Apodemus sylvaticus* (Linnaeus, 1758), *Myodes glareolus* Schreber, 1780, *Vulpes vulpes*, *Ursus arctos arctos* Linnaeus, 1758, *Meles meles* (Linnaeus, 1758), *Martes martes*, *Mustela putorius* Linnaeus, 1758, *Mustela erminea*, *Microtus nivalis*, *Lynx lynx* (Linnaeus, 1758), *Felis silvestris* Schreber, 1777, *Cervus elaphus*, *Capreolus capreolus* (Linnaeus, 1758), *Rupricapra rupicapra* and *Sus scrofa* (Wiszniowska, 1967, 1970, 1976, 1978, 1986, 1989; Marciszak, 2014, 2021; Marciszak et al., 2019, 2020, 2021, 2022, 2023, 2024b).

The importance of Jaskinia Niedźwiedzia (JN) is especially in the great abundance (+900,000 specimens) of well-preserved *U. s. ingressus* remains. This, the largest and most evolved cave bear subspecies, presents many distinctive morphological traits, suggesting a specialised vegetarian diet (Baca et al., 2012, 2014). The enormous abundance of well-preserved remains position JN as a pivotal reference for morphodynamic analyses in Central European populations. Compared to the type population of *U. s. ingressus* from Gamssulzenhöhle (Austria, MIS 3; Rabeder, 1983, 1995, 1999), the individuals from JN are larger. This is potentially influenced by factors like Bergman's rule, associated with the more northern setting of the locality. Morphodynamic analysis reveals a small degree of morphological variability and suggests the population's relative age during MIS 3 or 4. Radiocarbon dating places the age between 80–40 ka, signifying the earlier presence of this subspecies in the Sudetan region compared to Western Europe (Baca et al., 2012, 2014). Ancient DNA analysis confirms their assignation as *U. s. ingressus*. This population displays distinctive haplotypes considerably divergent from those in other European sites. This implies the probable isolation of *U. s. ingressus* population from JN from others (Marciszak et al., 2024b).

SYSTEMATIC PALAEONTOLOGY

Order Carnivora Bowdich, 1821
Infraorder Arctoidea Flower, 1869
Superfamily Ursoidea Fischer von Waldheim, 1817
Family Ursidae Fischer de Waldheim, 1817
Subfamily Ursinae Fischer de Waldheim, 1817
Genus *Ursus* Linnaeus, 1758
Ursus arctos Linnaeus, 1758
Ursus arctos taubachensis Rode, 1935
Ursus arctos arctos Linnaeus, 1758

D e s c r i p t i o n. – The material analysed from JN consists of 108 remains (NISP=108), belonging to at least 8 adult individuals (MNI=8). Four AMS dates documented the presence of two different brown bear subspecies, with *U. a. taubachensis* present between 51.7–42.2 ka cal BP and *U. a. arctos* occurring at 14.1–13.6 ka cal. BP (Table 1). The dates obtained generally fit into the general Eurasian trend of the presence of both subspecies, with *U. a. taubachensis* occurring during MIS 12-2 and *U. a. arctos* present since the end of MIS 2 until recently (Ersmark et al., 2019; Marciszak et al., 2020, 2022, 2024a). However, it cannot be completely ruled out that among hundreds of thousands of bones of young individuals and milk teeth of *U. s. ingressus*, there are also single, young specimens of *U. arctos*. However, the lack of clearly defined metric and morphological criteria distinguishing young individuals of both species makes it impossible to select them. The material of *U. arctos* is represented by fragments of both cranial and postcranial skeleton elements. The cranial material represents several mandibles and isolated teeth. The postcranial material consists mainly of long bones, metacarpals, metatarsals and phalanges. The state of preservation is good and allows all measurements to be carried out on the vast majority of specimens. The material has the exact location of the find and inventory numbers, which allows for precise identification of its position within the profile.

U p p e r d e n t i t i o n. – The P4 tooth is triangular, with the lingual, mesial and distal margins blunt, while the buccal margin is concave in the median part (Fig. 2A–C). Paracone is large, round and relatively low. The metacone is almost equal in size to the paracone, but lower, and more oval; the valley between them is strongly pronounced. An elongated, oval and low protocone is well developed, and sharply delineated from the remaining part of the crown. Its mesial margin forms a wide, open angle with the distal margin of the paracone. The cingulum is weakly developed, but stronger (forms a small crest) in the disto–buccal part of the crown. One specimen was assigned to the morphotype A/B, while two others were assigned to the morphotype B (Fig. 2A–C).

The square-shaped M1 is symmetrical in occlusal view, with a talon that is slightly longer and broader than the trigon (Fig. 2D–G). The mesial margin of the tooth is blunt to rounded, with a moderately expanded parastyle, while the distal margin is rounded. The buccal side is mostly straight, and it is moderately concave only at the transition between the trigon and talon. The lingual margin of the trigon is straight, while the lingual margin of the talon is expanded and rounded; a gentle, median concavity occurs between them. The low and triangular parastyle is moderately large, separated from the paracone and associated with the mesial cingulum. Its interior crest ends forming a cusp. The paracone and metacone are rounded, high and almost equal in size; the valley that separates them is deep. They are clearly separated from the buccal cingulum. The internal slopes of the paracone and the metacone have edges and pillars. The lingual cingulum is well-developed, collars the lingual slope of the protocone and terminates in the indentation between the mesocone and hypocone. The small metastyle is shallow and elongated, with a distal edge, and strongly associated with the distal cingulum. The mesocone is divided. The protocone is a low, rectangular cusp, on which internal wall are situated thick and sharp pillars and ribs (Fig. 2D–G).

T a b l e 1

Accelerator mass spectrometry (AMS) dates of *Ursus arctos* ssp. remains examined in this paper

Subspecies	Bone	Date	Lab. no.	^{14}C age	Cal BP 95.4%	Remarks	Source
U. a. arctos	mandible	AMS	Poz-82391	11950 ± 60	14045-13604	1.6% N, 9.1% C	(15)
U. a. taubachensis	mandible	AMS	Poz-82390	38200 ± 900	42459-42206	2.2% N, 13.3% C	(15)
U. a. taubachensis	humerus	AMS	Poz-82388	42200 ± 1500	45146-44556	1.9% N, 9.6% C	(15)
U. a. taubachensis	humerus	AMS	Poz-82387	47600 ± 2800	51717-48937	1.8% N, 6.5% C	(15)

The calibration was made with *OxCal* software version *OxCal v4.4.1* (Bronk Ramsey, 2021). Atmospheric data from Reimer et al. (2020). Calibrated dates are shown with 95.4% probability

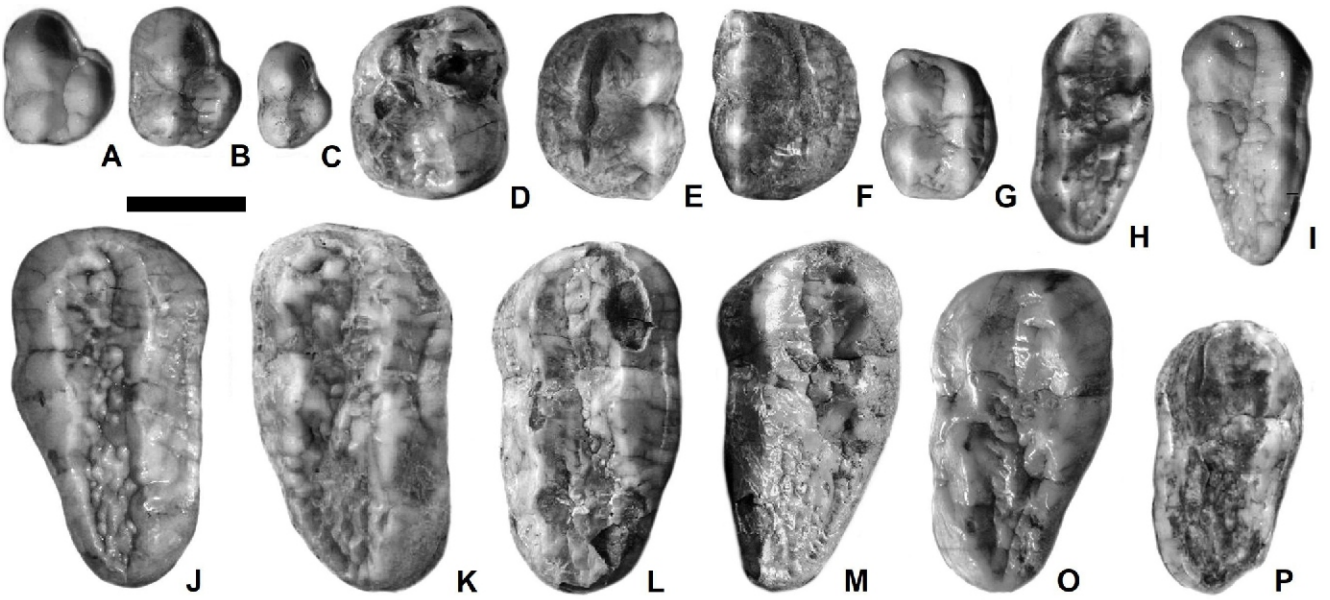

Fig. 2. The upper dentition of *Ursus arctos* from Niedźwiedzia Cave

Ursus arctos taubachensis: **A** – right P4 (JN.5.90), **B** – right P4 (JN.5.91), **D** – left M1 (JN.5.93), **E** – left M1 (JN.5.94), **F** – right M1 (JN.5.95), **J** – right M2 (JN.5.61), **K** – right M2 (JN.5.62), **M** – left M2 (JN.5.64), **N** – left M2 (JN.5.65), **O** – left M2 (JN.5.66), **P** – left M2 (JN.5.99). *Ursus arctos arctos*: **C** – right P4 (JN.5.92), **G** – right M1 (JN.5.96), **H** – left M2 (JN.5.97), **I** – right M2 (JN.5.98). All individuals shown at the same scale (scale bar = 20 mm) in occlusal view

Morphotype analysis: JN.5.91: paracone lingual wall – 2, metacone lingual wall – 2, lingual cingulum – 2, talon field – C, protocone wall – B2. JN.5.93: paracone lingual wall – 1, metacone lingual wall – 1, lingual cingulum – 2, talon field – C, protocone wall – B3. JN.5.94: paracone lingual wall – 2, metacone lingual wall – 2, lingual cingulum – 2, talon field – C, protocone wall – B2.

An elongated and rectangular M2 has all main cusps connected by a crest running by almost entire crown length and following the tooth outline (Fig. 2H–P). The trigon is expanded and broad, while the talon is elongated and narrows distally. The rounded, high paracone is located far from the metacone and separated from it by a shallow but distinctive valley. In JN.5.61 its mesial ridge is in contact with the mesial ridge of the protocone, forming a junction which is somewhat smooth. The next 4 teeth represent various variants of the morphotype B, which is characterised by the development of an additional side branch running on the mesio-lingual slope of the parastyle, but not reaching the base of this cusp. In addition, a mesial ridge of the parastyle formed a group of 4–5 cuspid-like structures that collar the mesial wall of the trigon. They yield 2–3 pillars on the internal wall of the paracone. These pillars start from the base of this cusp and reach half of its height. The metalophe complex is formed by a few (5–7) small cuspids located between the protocone and metacone, and the complex is pushed more distally. These cuspids run in disorder or order, one by one, from the metacone to the hypocone. In JN.5.64 the mesostyle complex forms (distal slope of the paracone and the mesial slope of the metacone) a double arch, the inner arm of which is strongly centrally curved into the lingual direction. In the next four teeth the distal arm of the paracone is considerably curved centrally, with a loose connection with the mesial arm of the metacone and forming a separate arch. In two M2, the posterolophe complex, located between the metastyle and hypocone, is created by a few (4–6) small cuspids, which do not form any regular lines, while in two others they occur in a regular line. The talon field is covered by numerous elongated cuspids and collared by a thick wall of distal cingulum, which forms numerous small cuspids. In two M2, metastyle and posthypocone are absent, while in three others they are developed into small and low cusps. The internal wall of the paracone consists of a few pillars and ribs, which start from the internal base of the protocone, but do not reach the apex. In two M2 they are stronger and thicker, and almost reach the apex. The lingual cingulum ends near the top of the hypocone in two M2, while in three others the cingulum reaches the incision between the hypocone and the posthypocone (Fig. 2H–P).

Morphotype analysis:

- JN.5.61: parastyle – B1, mesostyle – B3, metalophe – B2, metastyle/posthypocone – 2/2, lingual cingulum – 1.5.
- JN.5.62: parastyle – B1, mesostyle – B1, metalophe – B1, posterolophe – 2, talon field – C, paracone lingual wall – B, metastyle/posthypocone – 2/2, distal cingulum – C, protocone lingual wall – 1, lingual cingulum – 2.
- JN.5.64: parastyle – B1, mesostyle – B2, metalophe – C1, posterolophe – 1, talon field – B, paracone lingual wall – B/C, metastyle/posthypocone – 1/1, distal cingulum – B, protocone lingual wall – 1, lingual cingulum – 2.
- JN.5.65: parastyle – B2, mesostyle – B2, metalophe – C1, posterolophe – 2, talon field – C, paracone lingual wall – B/C, metastyle/posthypocone – 2/2, distal cingulum – C, protocone lingual wall – 1, lingual cingulum – 2.
- JN.5.66: parastyle – A3, mesostyle – A1, metalophe – B1, posterolophe – 1, talon field – C, paracone lingual wall – B, metastyle/posthypocone – 1/1, distal cingulum – B, protocone lingual wall – 1, lingual cingulum – 1.5.

M a n d i b l e. – The most spectacular find from JN is the left mandible of a giant individual (JN.5.1). This is the only specimen of *U. arctos* previously described (although only briefly) from this site (Wiszniowska, 1970, 1989). It has already been noted that only the c1 is missing, from the strong degree of wear, with simultaneous slight wear of the molars (Wisz-

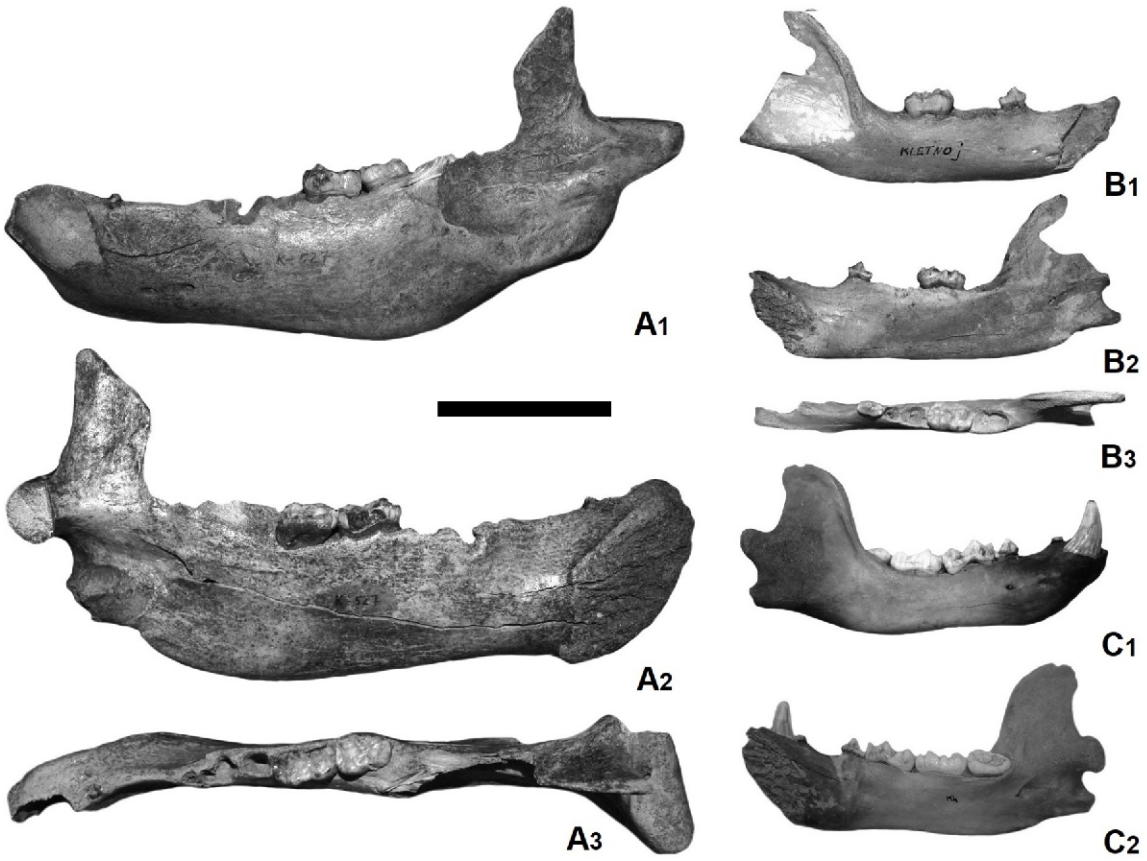

Fig. 3. Mandibles of *Ursus arctos* from Niedźwiedzia Cave

Ursus arctos taubachensis: **A** – left (JN.5.1). *Ursus arctos arctos*: **B** – right (JN.5.2), **C** – right (JN.5.100).
All individuals shown at the same scale (scale bar = 100 mm), 1 – buccal view, 2 – lingual view, 3 – occlusal view

niowska, 1970, 1989). The mechanism of this phenomenon itself is unclear. It may have been a malocclusion, or the water flowing through the cave may have played a certain role in grinding the crown; it is difficult to say unequivocally. The mandible is missing a large part of the ramus, as well as most of the teeth, of which p1, m2 and m3 are preserved (Fig. 3).

The first feature is its particular size, exceeding all previously known specimens. What is more, it belongs to a specimen that was not yet fully grown, probably several years old, its total length being close to 355 mm. Judging from the degree of development of the alveoli and symphysis, the value of this measurement for a fully grown individual could reach 380–400 mm. Comparing it with the size for other large brown bears from the Pleistocene of Europe, it becomes clear how huge this male specimen was. The total length of the mandibles of other large specimens is usually in a range below 300 mm. However large individuals, with mandible sizes between 300–340 mm, are not commonly but regularly found at European sites (Gunther, 1923; Torres Pérez Hidalgo, 1988a, Marciszak et al., 2021, 2023, 2024a). For comparison, the mandible length of the Holocene and extant *U. a. arctos* from Europe rarely exceeds 250 mm (Jakubiec, 1993; Baryshnikov, 2007). The rounded masseteric fossa, reaching the distal edge of the m3 alveoli, is shallower and lacks the characteristic (for *U. s. ingressus*) flattening of the lower part, which is the place of attachment of the powerful chewing muscle. The mandibular body, elongated and massive, is, however, more slender than the mandibular body of *U. s. ingressus*. Its height and massiveness increase from the symphysis towards the ramus, reaching its maximum dimensions at the height of m3. A characteristic feature of *U. a. taubachensis*, which can be considered one of its diagnostic features, is a strongly marked curvature of the lower margin of the mandibular body. This feature is also present in *U. spelaeus*, as well as in the large coastal bears from the Bering Sea (Baryshnikov, 2007). This feature is poorly developed in postglacial individuals and often absent in Holocene or extant European individuals (Fig. 3). The dentition has a formula typical of *U. arctos*. The teeth row is straight, the teeth are set closely together and are separated only by small diastemas. All premolars (p1–p3) are present, a feature typical of a brown bear. In *U. spelaeus*, additional premolars are found only exceptionally and usually in single numbers (Pacher, 2017). The preserved p1 is a strongly reduced, one-rooted tooth, separated from the canine by a diastema. The alveoles of p2 and p3 also indicate small, rounded and reduced teeth.

The mandible JN.5.3 is characterised by a morphology similar to the above-noted specimen, but the degree of preservation is poorer. It belongs to a fully grown male, and its estimated length could have been ~370–380 mm, similarly to specimen JN.5.1. Apart from the large size, the sex is also clearly indicated by the massive alveoli of the canine tooth. Its morphology includes features also found in the hemandible JN.5.1, which characterize *U. a. taubachensis*, like the large size, massive and elongated symphysis (more slender than *U. spelaeus*), strongly marked curvature under m3, the lack of a surface in the lower part of the massteric fossa for muscle attachments, and the presence of alveoli after p1–p3.

The right mandible (JN.5.2) belongs to a young adult, a female ~3 years old, as indicated by the narrow alveola of the canine and its small size. Its young age is indicated by the incom-

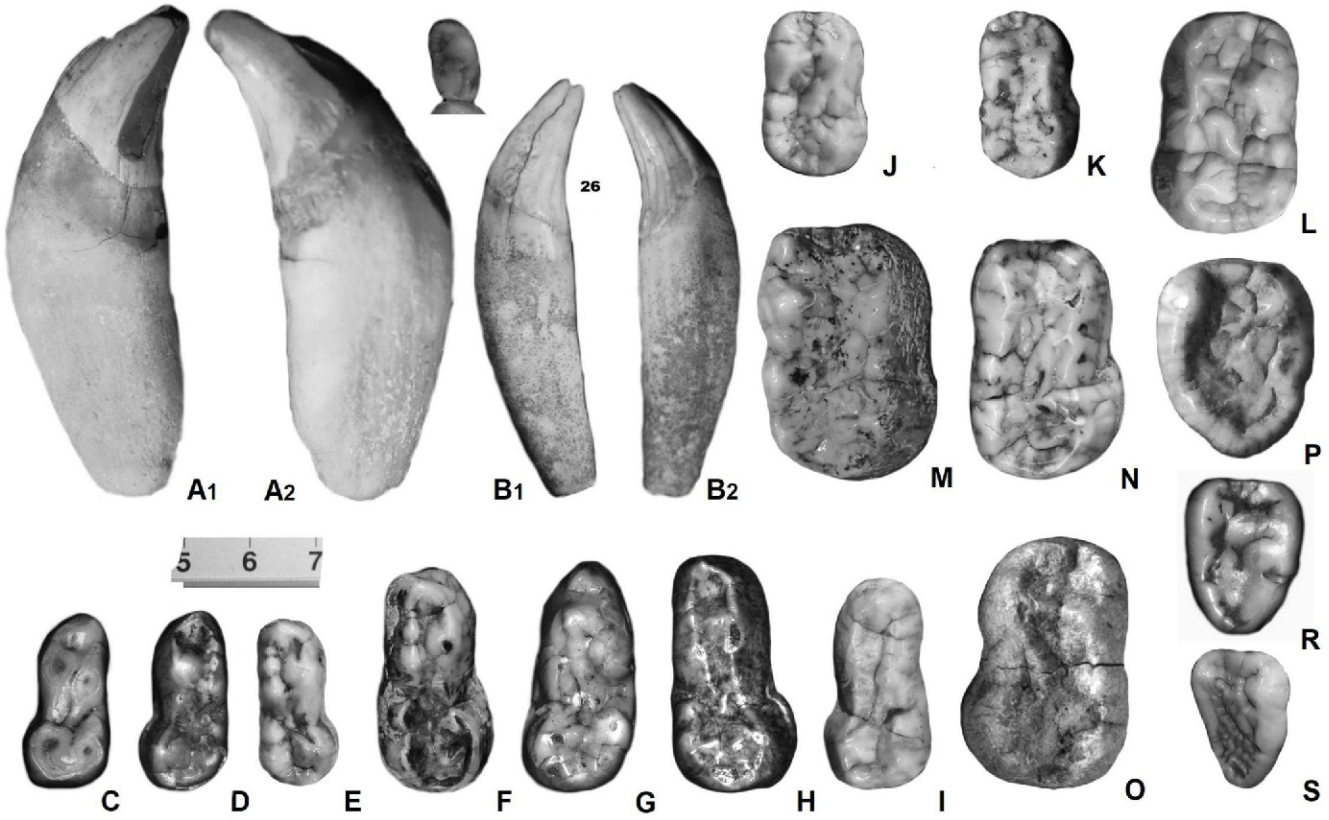

Fig. 4. Lower dentition of *Ursus arctos* from Niedźwiedzia Cave

Ursus arctos taubachensis: **A** – left c1 (JN.5.47), **B** – left c1 (JN.5.48), **F** – right m1 (JN.5.60), **G** – left m1 (JN.5.63), **H** – right m1 (JN.5.101), **I** – left m1 (JN.5.102), **L** – left m2 (JN.5.103), **M** – right m2 (JN.5.54), **N** – right m2 (JN.5.67), **P** – right m3 (JN.5.55). *Ursus arctos arctos*: **C** – left m1 (JN.5.52), **D** – left m1 (JN.5.53), **E** – right m1 (JN.5.100), **J** – right m2 (JN.5.100), **K** – right m2 (JN.5.2), **R** – right m3 (JN.5.104), **S** – right m3 (JN.5.100). All individuals shown at the same scale (scale bar = 10 mm). Specimens A and B: 1 – buccal view, 2 – lingual view. All other teeth (C–S) shown in the occlusal view

pletely developed condylar and angular processes. The specimen had not yet reached its full size, although its size will not change significantly and the total length would be ~230 mm. This size is within the range of variability of extant *U. a. arctos* females from Central Europe (Jakubiec, 1993). The morphology of the specimen is characterised by a set of features typical of *U. a. arctos* like a short and narrow symphysis, proportionally long diastema between p1 and p4 and a shallow and short masseteric fossa. The occurrence of two other features is symptomatic, characterising the evolutionarily advanced form *U. a. arctos*, and not found or occurring only rarely in *U. a. taubachensis*. First is the loss of additional premolars (in specimen JN.5.2 only alveola p1 is present), a feature characteristic of Holocene and extant European individuals (Nagel, 2017). The second is the almost straight lower margin of the mandibular body, and lack of curvature under m3 (Fig. 3).

Lower dentition. – Apart from their size, the canines are of little use in taxonomic analyses due to the lack of diagnostic features. They are smaller and more slender with proportionally longer crowns than the canines of *U. spelaeus*. The C1 is characterised by a longer and straighter crown than c1, and it also lacks a specific keel, present on the lingual side of c1. The cingulum surrounding the crown and clearly separating itself from the root is formed as a low, flattened collar. Although the sexual dimorphism is less clearly expressed than in *U. spelaeus*, the canines of males are distinctly larger and more robust than those of females (Fig. 4A, B).

Apart from the rudimentary p1 in the hemimandible JN.51, there are no preserved additional premolars in the material analysed. The present alveoles indicate extremely reduced, oval or rounded, one-rooted teeth. Three preserved, isolated p4 (JN.5.68, JN.5.69 and JN.5.70) are characterised by a simple structure and small size. The oval crown has a low apex with a rounded top, and edges running from it in mesial and distal directions. The crown is surrounded by a thin cingulum. There are no additional cuspulids or structures on the surface of their crowns. Three other p4, two in the hemimandibles (JN.5.2, JN.5.50) and the isolated JN.5.51, are characterised by a similar morphology, typical of *U. a. arctos*. These proportionally small teeth, with narrow and low crowns, represent the b1 morphotype. The protoconid is located centrally and from its apex there run mesially and distally two narrow but clearly defined edges. Near the top of the protoconid, slightly shifted disto-mesially, there is a small but clearly defined metaconid. The entire crown is surrounded by a poorly marked, low cingulum. In JN.5.2 and JN.5.51 the distal cingulum is definitely thicker.

m1. The main cusps of the m1 are connected to each other by a crest, which follows the outline of the tooth (Fig. 4C–I). In occlusal view, the tooth is elongated, and has a moderately expanded talonid. The mesial margin of the trigonid is rounded, the lingual one is straight, while the buccal is almost straight, with a gentle concavity at the level of the protoconid. The broader talonid has a straight lingual margin, strongly convex

buccal and rounded or blunt distal margins. The apex of the triangular and low paraconid is oriented slightly mesially. Situated behind, the rectangular protoconid is the highest and largest cusp, with an almost vertical apex. Both main cusps are separated by a wide, V-shaped valley. On the lingual side of the trigonid, a triple metastylid is situated. A relatively high, elongated and rectangular metaconid is situated after the metastylid. The lingual half of the talonid is occupied by a double or triple entoconid, square-shaped to rectangular, and relatively low cusps, situated one after the other. On the internal slopes of the entoconids there are a few thick and strong pillars and ribs. The entyphoconid is well developed; however, it is separated from the hypoconid by a thick ridge in some individuals. In the remaining three teeth it formed an irregular structure. The talonid cusps are relatively close. The distal end of the talonid possesses a double entyphoconid and hypoconulid (Fig. 4C–I).

Morphotype analysis of m1:

- JN.5.102: entoconid – B3, entoconid pillar – C, distal ridge – 3, enthypoconid – B.
- JN.5.103: metastylid – 3, entoconid – B2, entoconid pillar – D, distal ridge – 3, enthypoconid – C.
- JN.5.52: metastylid – 3, entoconid – B4, entoconid pillar – C, distal ridge – 3, enthypoconid – C.
- JN.5.60: metastylid – 1, entoconid – A2, entoconid pillar – A, distal ridge – 2, enthypoconid – A.
- JN.5.63: metastylid – 3, entoconid – A2, entoconid pillar – A/B, distal ridge – 3, enthypoconid – B.
- JN.5.53: metastylid – 1, entoconid – A2, entoconid pillar – A/B, distal ridge – 3, enthypoconid – B.

m2. The m2 vary in size, but are within the range of variation of *U. a. taubachensis*. Mesial and distal margins are gently rounded or blunt, the lingual margin is straight, moderately concave in the middle part, in the transition between the trigonid and talonid (Fig. 4J–O). The buccal margin of the trigonid is slightly rounded, while that from the talonid is moderately expanded and rounded. The occlusal surface is highly complicated. On three m2s the metalophid has, on the internal slope of the protoconid, an additional cuspid, entprotoconid, which is connected with the metaconid by the cutting edge. In two others on the metalophid two additional cuspids are present: entprotoconid and entmetaconid. The entprotoconid is separated from the protoconid by a wide and shallow furrow. The internal field of the trigonid has 1–3 small, clearly recognisable cuspids and few thick, well-developed furrows and pillars. The metastylid is simply built, with two larger cuspids, one mesially and one distally. The mesolophid complex is moderately developed. It is developed as a clearly visible, thick and dominant ridge or wall, which starts from the disto-lingual slope of the protoconid, running through the trigonid and the talonid boundary and ending lingo–medially on the internal field of the talonid. The entyphoconid is variably developed, in JN.5.1 it is present as a prominent, thick, quadruple groove, and is separated from the hypoconid by a wide ridge. In two others the strong entyphoconid is not divided and constitutes a prominent structure. Three m2 have the entyphoconid split into two parts. The hypoconulid is not present (Fig. 4J–O).

Morphotype analysis of m2:

- JR.5.103: metalophid – C, trygonid – 2, metastylid – 2, mesolophid – B, enthypoconid – C, hypoconulid – 1.
- JR.5.67: metalophid – C, trygonid – 2, metastylid – 2, mesolophid – B, enthypoconid – C, hypoconulid – 1.
- JR.5.3: metalophid – B, trygonid – 2, metastylid – 2, mesolophid – B, enthypoconid – B/C, hypoconulid – 1.
- JR.5.1: metalophid – B, trygonid – 2, metastylid – 1, mesolophid – A, enthypoconid – B, hypoconulid – 1.
- JR.5.2: metalophid – C, trygonid – 1, metastylid – 2, mesolophid – A, enthypoconid – A, hypoconulid – 1.
- JR.5.54: metalophid – C, trygonid – 3, metastylid – 2, mesolophid – B, enthypoconid – B/C, hypoconulid – 1.

m3. In occlusal outline two m3 are oval in shape, with a weakly marked buccal concavity and sharper distal margin of the crown (Fig. 4P–S). Two others are more irregular and broader, with a more strongly developed talonid. The protoconid complex has a shifted lingually and extending transversally mesolophid, with two small cuspids and one thin pillar. In two m3 the hypoconid is simply built, with a few thin, short ridges and pillars. The centrolophid is present as a series of small and low cuspids running disto-buccally from the metaconid base to the buccal slope of this cusp. It is connected with the mesolophid by a thin and sharp ridge. The entoconid occurs as a series of moderately large and low cuspids, arranged one behind the other, and two among these cuspids are enlarged. The talon field is complicated and holds a few moderately large cuspids (Fig. 4P–S).

The morphology of JN.5.1 and JR.5.54 have a morphology typical of *U. a. taubachensis*, of great size, massive structure and a complicated chewing surface. The crown is large and wide, its dimensions significantly exceeding those of Holocene and extant *U. a. arctos*. They are characterised by an irregular shape (morphotype B), with a clearly marked transition of the trigonid to the talonid on the buccal side. The trigonid is significantly longer and wider than the talonid, which is wide compared to that of *U. a. arctos*. The protoconid complex is moderately developed (morphotype B3), lacking the mesolophid, with one thicker, smooth groove running from the top of the protoconid towards the base of the metaconid. Additionally, there are 2 narrow, delicately marked lines on its surface. On the inner surface of the metaconid there is a small, strongly associated cuspulid (morphotype B). The hypoconid is relatively weakly marked, with three narrow grooves (morphotype B3). The centrolophid is present in the form of several small, low but clearly defined cuspulids, running in a buccal direction from the base of the metaconid to the base of the hypoconid (morphotype B). A line of several peripherally located, lingually located cuspulids, and the presence of two larger cuspulids, which could be treated as entoconid (morphotype C). The chewing surface of the talonid has a complex structure, with 7 cuspulids of different size and several grooves (morphotype D).

The typical m3 *U. a. arctos* is a comparatively small tooth, with an oval crown, regularly tapering towards the back. The protoconid and metaconid are morphologically similar, low forms with a flattened crown. The chewing surface has relatively simple morphology. Two m3 from JN (JN.5.55, JN.5.1) have oval crowns, evenly tapering towards the back (morphotype A). The low protoconid complex forms an elongated, triple-branched mesolophid, directed disto-lingually (morphotype A2). The inner wall of the metaconid lacks an additional cuspulid (morphotype A). The hypoconid is poorly developed in the form of two narrow, low edges, directed mesiomedially (morphotype B2). The centrolophid is fragmentary, developed in the form of several cuspulids (morphotype A). The entoconid complex is formed by several small cuspulids, located one behind the other on the lingual edge of the talonid (morphotype B), the chewing surface of which is flat (morphotype B). The talonid is elongated, but relatively narrow (Fig. 4P–S).

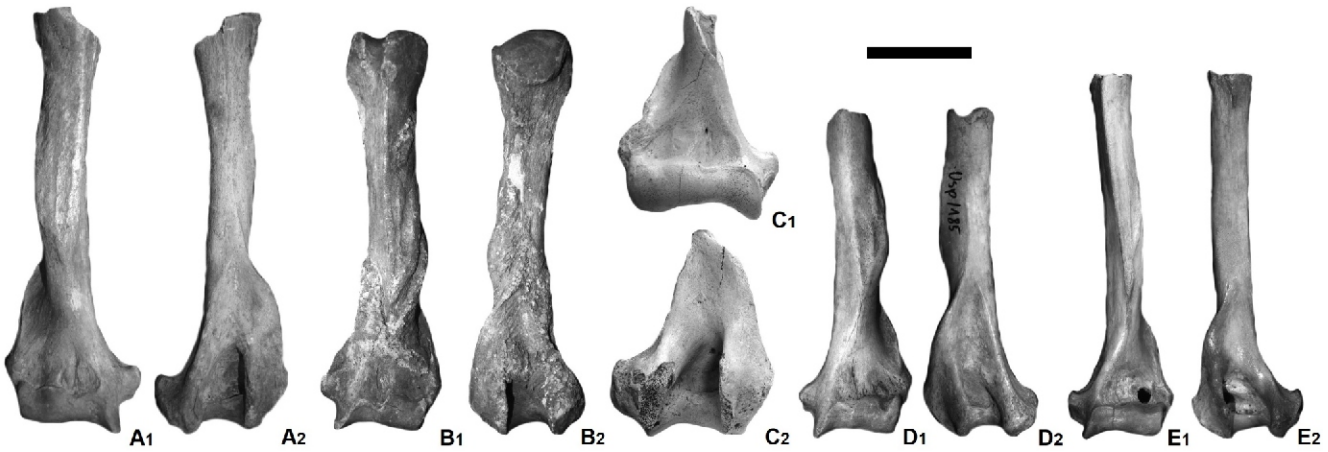

Fig. 5. Humerus of *Ursus arctos* from Niedźwiedzia Cave

A – right (JN.5.59), **B** – left (JN.5.58), **C** – right (JN.5.88), **D** – left (JN.5.89), **E** – left (JN.5.87). All individuals shown at the same scale (scale bar = 100 mm), 1 – dorsal view, 3 – ventral view

Long bones. All long bones (except humerus JN.5.72) belong to large and very large individuals, within the range of variability of the Holocene and extant *U. arctos*. JNK/Ua/7 is a true giant, the breadth of the distal epiphysis being ~179 mm, which allows for an estimated total length of between 580–600 mm (Fig. 5). With these dimensions, it is significantly above the range of variability of the contemporary brown bear from Europe. At the same time, this specimen is within the range of variability of large cave bears and the largest *U. s. ingressus* and *U. a. taubachensis* (Thenius, 1956; Bonifay, 1966; Kosintsev et al., 2019). The morphology of all humeri showed typical arctoid features, with a proportionally longer, more slender and more curved shaft and U-shaped proximal epiphysis (instead of V-shaped in *U. s. ingressus*). Additionally, the shaft is more slender, the muscle attachments are more strongly developed and the distal epiphysis is trapezoidal with both condyles ending sharply (Petronio et al., 2003).

Three complete ulnae, one small (JN.5.15, L 314 mm), one larger (JN.5.16, L=385 mm) and one very large (JN.5.65, L 447.7 mm), demonstrated the most probably strongly pronounced sexual dimorphism (JN.5.16 – ♀, JN.5.16 – ♂) and difference in size between *U. a. taubachensis* (JN.5.16, JN.5.65) and *U. a. arctos* (JN.5.15; Fig. 6). Ulna JN5.65 is very large, but much larger ulnae, exceeding 500–520 mm, are known (Kurtén, 1956, 1959, 1964; Janossy, 1963; Bonifay, 1966; Ingólfsson and Wiig, 2008). However, due to their specific structure (slender and fragile distal epiphysis), which significantly affects the probability of preservation in cave deposits, finds of complete ulnae are relatively rare compared to those of other long bones. All three ulnae from JN can be distinguished from those of *U. s. ingressus* in their more slender and strongly curved shape, stronger marked olecranon, triangular shaft in cross-section and more strongly curved distal epiphysis. A single complete radius (JN.5.5) from JN belongs to a medium sized (L 295 mm) individual, which differs from *U. s. ingressus* in a more slender structure and a more strongly curved shape, a narrower shaft without a triceps muscle attachment running along it, and wider and more massive epiphyses (Fig. 6).

Similarly to the ulnae, three intact tibiae from JN demonstrated the presence of three size classes, with the smallest one (JN.5.15) representing a female *U. a. arctos*. A medium-sized specimen (JN.5.66, L=346 mm) was assigned as a female, and a giant individual (JN.5.84, L=449 mm) as a male of *U. a. taubachensis*. All three tibiae showed the presence of arctoid features, and are distinguished from *U. s. ingressus* in their slender build and less massive proximal epiphysis, with more pronounced muscle attachments. Additionally, the ridge running from the proximal epiphysis almost reaches the distal epiphysis, while in *U. s. ingressus* it only reaches half the length (Petronio et al., 2003).

Tarsals. The most outstanding metrically (L=127 mm) and morphologically is a giant calcaneus (JN.5.105; Fig. 7A). The triangular medial process is broad and short. It is situated almost vertically to the corpus which is very massive in the mesio-distal direction. Almost the entire surface of the medial process is covered by an oval, broad and shallow facies articular astragali medialis. The lateral process forms a thin and high crest running from the distal end to halfway along the corpus. Running transversally, the broad and shallow facies articular astragali lateralis is separated from the facies articular astragali medialis by a deep and wide groove. An oval and deep facies articular cuboidea is connected distally with the facies articular astragali medialis. The crescentic and flat sulcus tendinis musculi flexoris hallucis longis is elongate and medially widened. Two other and smaller calcanei (JN.5.19 and JN.5.20) show similar morphology, and together with JN.5.105 were assigned to *U. a. taubachensis* (Fig. 7E, F). In comparison to the single calcaneus of *U. a. arctos* (JN.5.106), they differ by the following features: (1) larger size; (2) the medial process is elongate and rectangular, with the distal end oriented more medio-proximally; (3) the facies articular astragali medialis placed on the medial process is rectangular, rather flat and its margin forms a thin but sharply pointed ridge, which collars the whole surface; (4) the lateral process is more pronounced, the flat facies articular astragali medialis being longer and running more obliquely and (5) the facies articular cuboidea is shallower and does not contact with the facies articular astragali medialis (Fig. 7E, F).

Both complete talii (JN.5.21, JN.5.22) are characterised by arctoid features (Fig. 7B, C), where the sulcus tendinis musculi flexoris hallucis longi is proportionally almost twice as narrow as that of *U. s. ingressus* (Rabeder et al., 2010). The lateral edges of the trochlea in JN talii run almost parallel, while in *U. s. ingressus*, the medial edge slopes from medio-distally to lateral-distally and forms a steep angle with the expansion of the lateral edge (Fig. 7B, C). The inclination of the medial edge of

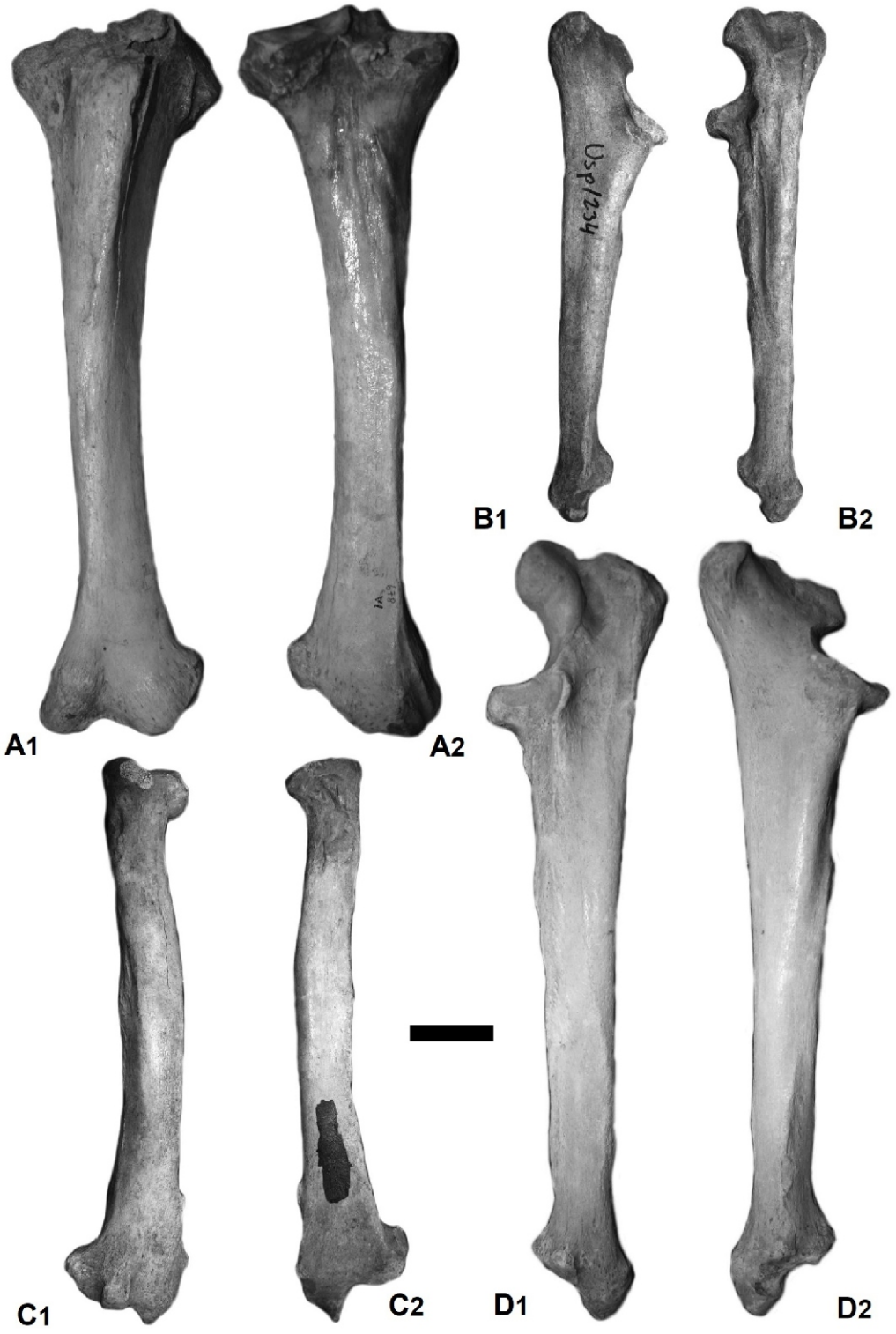

Fig. 6. Long bones of *Ursus arctos* from Niedźwiedzia Cave

Ursus arctos taubachensis: **A** – right tibia (JN.5.86), **D** – right ulna (JN.5.84). *Ursus arctos arctos*: **B** – right ulna (JN.5.6), **C** – right radius (JN.5.5). All individuals shown at the same scale (scale bar = 100 mm). Specimen A: 1 – dorsal view, 3 – ventral view, specimens B–D: 1 – medial view, 2 – lateral view

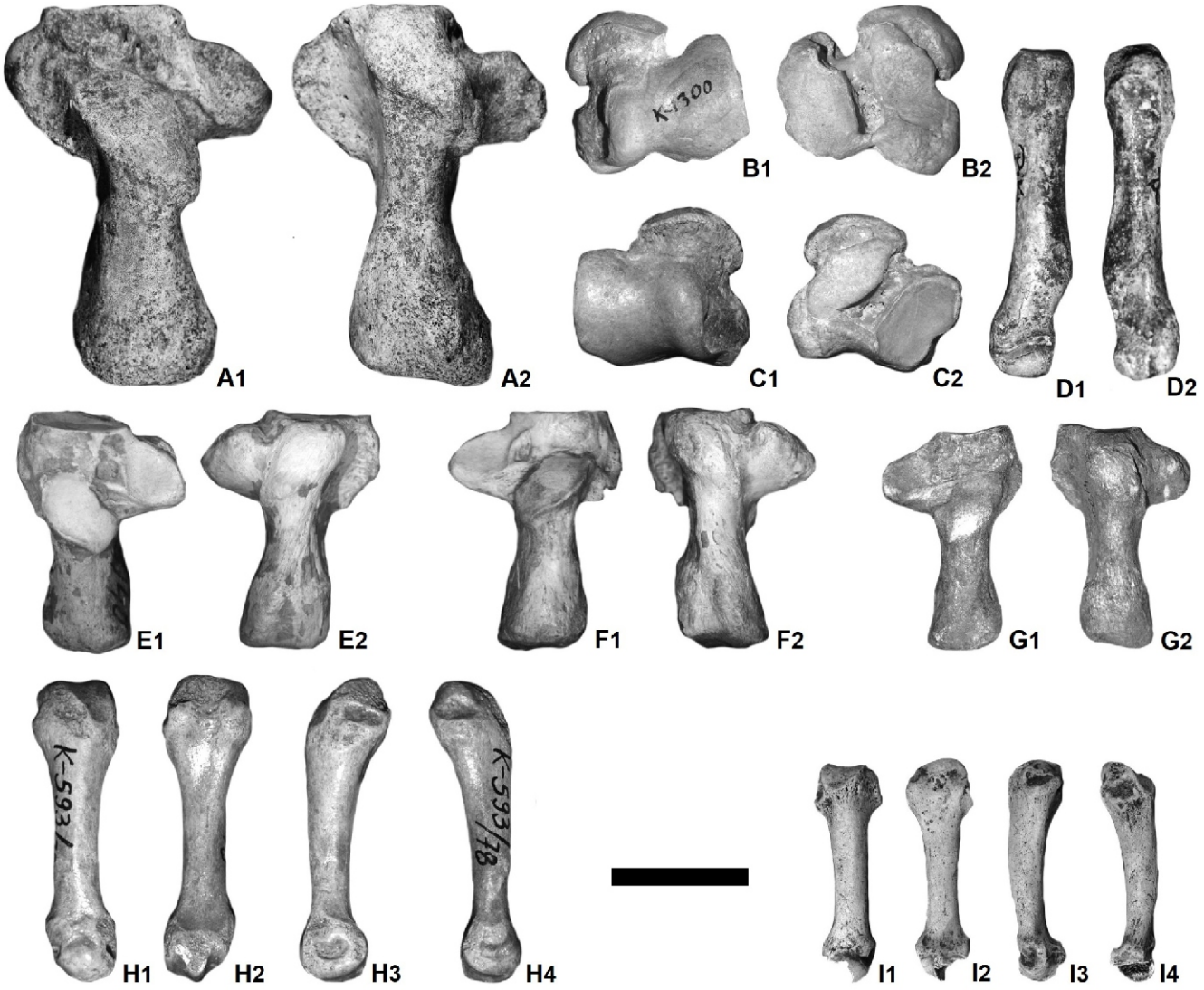

Fig. 7. Calcanei, metapodials and tali of *Ursus arctos* from Niedźwiedzia Cave

Ursus arctos taubachensis: **A** – left calcaneus (JN.5.105), **B** – right talus (JN.5.8), **C** – left talus (JN.5.9), **D** – right metatarsal 4 (JN.5.107), **E** – left calcaneus (JN.5.10), **F** – right calcaneus (JN.5.11), **H** – left metacarpal 1 (JN.5.72). *Ursus arctos arctos*: **G** – right calcaneus (JN.5.106), **I** – right metacarpal 1 (JN.5.22). All individuals shown at the same scale (scale bar = 50 mm), 1 – dorsal view, 2 – medial view, 3 – ventral view, 4 – lateral view

the trochlea is connected to the sprain of the tibia distal epiphysis (Rabeder et al., 2010). The specimens from JN are also smaller than astragali of *U. s. ingressus*.

Metapodials. In the analysis of bear evolution, two coefficients play an important role: the width of the shaft to the total length and the width of the distal epiphysis to the total length. Morphologically, all metapodials from JN are similar to those of *U. a. taubachensis* and differ from those of *U. a. arctos* in their proportionally more robust epiphyses and shorter and more massive shaft. Simultaneously, they are longer and more slender than those of *U. s. ingressus*. Their average values are almost equal to those of *U. a. taubachensis* and large coastal extant subspecies such as *Ursus arctos beringianus* Middendorff, 1851, *Ursus arctos lasiotus* Gray, 1867 and *Ursus arctos middendorffi* Merriam, 1896 (Baryshnikov, 2007).

Metacarpal 1 (mc 1). The proximal articulation surface of mc 1 for the carpale 1 is shaped into a saddle-like form (Fig. 7H, I). In the area of the medial epiphysis, there is a relatively wide fovea. The distal trochlea slopes from the mesio-distal towards the disto-proximal direction. The articular surface of the proximal epiphysis for metacarpal 2 is slightly convex and shaped like a small saddle. It extends obliquely outwards and downwards on the dorsal surface, forming a shallow articular fossa in which the thumb moves freely in the transverse direction. There is a small articular surface on the inner edge. Similarly, there is also an articular surface on the outer side, which rests on the inner edge of mc 2. The narrow shaft has an oval cross-section and is slightly curved at both ends. It is slightly bent outwards, and on its dorsal surface there is a groove running from the outer edge obliquely outwards and forwards. This is a strongly developed attachment for the extensor. The concave palmar surface is strongly folded for attachment of numerous ligaments. The oblique distal articular surface is turned inwards and downwards. Just above it, in the middle of the palmar surface, is a well-defined, small tubercle that provides attachment to a ligament of the bone connecting with the first phalanx of the second row and to the thumb muscle (Fig. 7H, I).

Metacarpal 2 (mc 2). The mc 2 is short and bulky (Fig. 8B). The tuberculum medial is well-developed. It appears proportionally shorter and more massive than mtcp I. The proximal

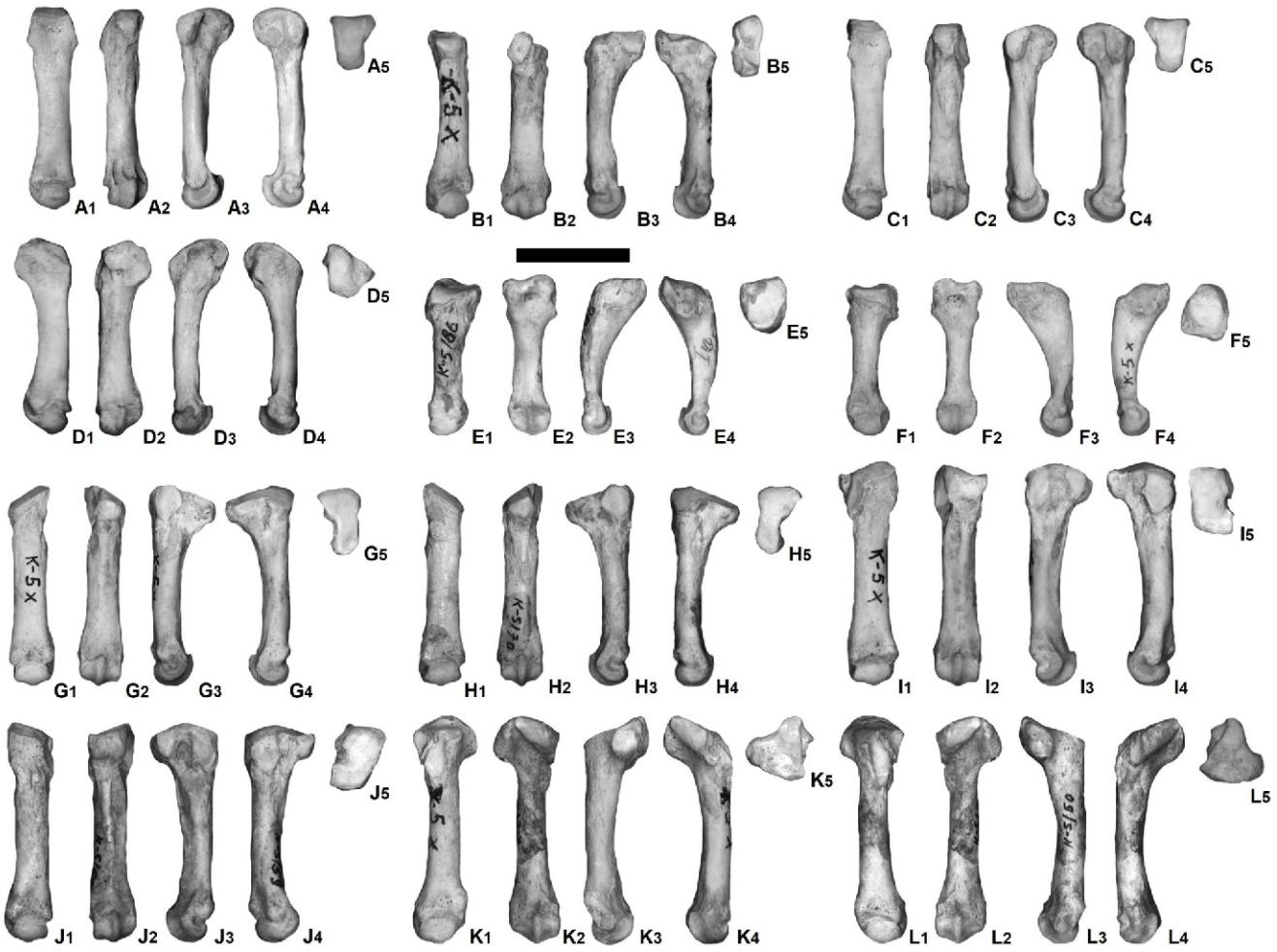

Fig. 8. Metapodials of *Ursus arctos taubachensis* (one individual) from Niedźwiedzia Cave

A – left metacarpal 4 (JN.5.82), **B** – left metacarpal 2 (JN.5.73), **C** – right metacarpal 4 (JN.5.108), **D** – right metacarpal 5 (JN.5.26), **E** – right metatarsal 1 (JN.5.21), **F** – left metatarsal 1 (JN.5.20), **G** – left metatarsal 3 (JN.5.32), **H** – right metatarsal 3 (JN.5.31), **I** – left metatarsal 4 (JN.5.35), **J** – left metatarsal 2 (JN.5.28), **K** – left metatarsal 5 (JN.5.19), **L** – right metatarsal 5 (JN.5.24). All individuals shown at the same scale (scale bar = 50 mm), 1 – dorsal view, 2 – medial view, 3 – ventral view, 4 – lateral view, 5 – proximal view

wedge-shaped epiphysis has slightly outwardly shifted edges. It is rectangular in front, while a small tubercle is present at the back, on the palmar surface. The trapezoidal articular surface is triangular in outline, concave transversely and almost flat vertically. There is a small flat surface on the upper and outer edge, which connects posteriorly with the capitate bone. Above it is another triangular surface set at right angles to the shaft, bordering the anteriorly inner surface of the capitate bone. The anteriorly inner part of the trapezoidal surface contains a small, concave surface, which contacts the convex outer surface of the trapezoid bone (trapezoideum). This area, extending posteriorly, is a broad, slightly concave contact surface with mc 1. Below the articular surfaces for the capitate are two concave surfaces, anteriorly larger and deeper, which overlap the corresponding surfaces on the ventral side of mc 3. On the anterior surface of the proximal epiphysis, a shallow groove runs obliquely to its upper part, which is attached to the ligament of the trapezium. The entire head of mc 2 is roughened for the attachment of the ligaments of the carpal bones and adjacent metacarpals. The relatively narrow shaft is triangular in cross-section at the proximal epiphysis and almost circular in the middle and distal directions. The massive distal epiphysis is separated from the shaft by deep dorsal and lateral depressions (Fig. 8B). On the inferior surface, there is a short ridge in the midline. This fits into the notch on the distal epiphysis of the first phalanges. On both sides of its base are sesamoid bones, to which almost all the flexor tendons of the adductor and the muscles moving the metacarpals are attached. At the point where the shaft joins the distal epiphysis there is a tuberosity, which encompasses the sides of the phalangeal joints. In general appearance, the distal articular surface is almost straight on the inside and strongly curved on the outside (Fig. 8B).

Metacarpal 3 (mc 3). The proximal articulation of mc 3 is set nearly at a right angle to the end of the shaft (Fig. 8). The dorsal face expands considerably more than the distal face. It is vertically convex, transversely concave. There is a broad oval surface set on its inner side. These two articular surfaces are divided from each other by a well-marked ridge. On the external side, there are two concave surfaces, which overhang and articulate with mc 4. They are deeply concave and are more confluent than those of mc 2. On the mesial surface, a shallow groove of the proximal epiphysis runs diagonally and a trapezoidal ligament was attached to its upper part. The entire head of the bone is roughened for the reception of the ligaments binding the bone to the carpus and its fellow metacarpals. The shaft presents a triangular section proximally, and it is nearly circular in the mid-

Table 2

Basic measurements and indices of *Ursus arctos* ssp. metacarpals analysed in this paper

		JN			*U. a. taubachensis*			*U. a. arctos*		
		M	Min-Max	N	M	Min-Max	N	M	Min-Max	N
mc 1	GL	80.99	70.35–92.79	4	82.68	67.65–96.56	50	67.68	51.49–77.89	58
	TI	17.7	17.1–18.6	4	17.6	14.9–21.9	50	14.3	11.6–16.4	58
	PI	27.5	25.1–29.7	4	27.2	24.1–32.7	50	23.9	20.7–29.5	58
mc 2	GL	78.56	71.28–88.54	4	87.44	71.28–105.68	49	75.64	62.23–88.34	56
	TI	18.9	18.1–19.5	4	18.1	16.3–19.6	49	15.2	12.6–17.5	56
	PI	30.8	27.7–33.4	4	28.0	17.9–33.7	49	23.7	16.4–28.8	56
mc 3	GL	85.68	82.92–88.34	3	90.11	77.78–113.16	59	78.15	63.49–97.55	53
	TI	17.7	17.2–18.2	3	17.9	15.1–20.2	59	14.7	12.4–17.8	53
	PI	26.8	23.2–27.9	3	27.5	23.2–32.2	59	23.2	19.1–28.2	53
mc 4	GL	90.64		1	93.25	81.56–121.97	42	80.27	66.75–96.84	57
	TI	19.1		1	17.8	14.3–20.5	42	15.3	13.5–16.7	57
	PI	28.3		1	27.1	23.4–31.3	42	23.3	20.9–27.1	57
mc 5	GL	96.89	85.49–113.69	4	96.68	84.49–113.69	49	82.19	66.49–99.78	65
	TI	16.9	16.1–17.5	4	18.6	16.1–22.1	49	15.5	13.9–17.1	65
	PI	27.9	26.1–30.9	4	28.5	24.5–32.8	49	24.7	18.3–28.4	65

Table 3

Basic measurements and indices of *Ursus arctos* ssp. metatarsals analysed in this paper

		JN			*U. a. taubachensis*			*U. a. arctos*		
		M	Min-Max	N	M	Min-Max	N	M	Min-Max	N
mt 1	GL	75.33	69.57–83.27	3	76.34	65.04–86.59	42	65.91	51.55–87.67	55
	TI	18.7	17.5–19.6	3	17.6	13.7–20.1	42	15.4	13.2–16.6	55
	PI	28.3	25.8–30.1	3	28.2	24.5–32.1	42	24.8	20.2–29.9	55
mt 2	GL	80.88		1	86.29	71.67–109.88	49	72.14	57.55–89.97	51
	TI	18.1		1	18.2	15.2–21.2	49	15.3	12.4–16.6	51
	PI	29.6		1	27.3	24.1–31.2	49	24.6	20.7–28.4	51
mt 3	GL	87.28	83.44–90.02	5	89.43	68.32–114.64	60	79.45	70.56–99.75	58
	TI	18.4	17.9–18.8	5	18.1	16.1–20.1	60	15.4	13.9–16.9	58
	PI	28.2	24.8–27.8	5	25.5	21.7–28.9	60	22.7	19.5–25.4	58
mt 4	GL	98.68	91.74–106.24	5	100.81	86.34–116.78	62	85.56	71.55–106.24	65
	TI	17.8	16.9–18.7	5	17.6	16.1–19.4	62	15.7	13.9–16.6	65
	PI	24.3	21.7–26.1	5	24.4	21.7–27.4	62	22.1	19.1–26.9	65
mt 5	GL	97.86	83.11–110.48	6	99.64	83.11–118.67	57	87.75	70.56–99.94	62
	TI	15.8	14.8–16.8	6	16.5	14.3–18.3	57	13.1	11.7–15.8	62
	PI	26.7	23.9–28.3	6	24.5	21.3–28.3	57	22.2	18.7–25.5	62

dle and distally. A slight palmar ridge is developed behind, at the point where it joins the distal articulation, and it is flattened in front. The distal epiphysis is bulb-shaped, and divided from the epiphyseal line of the shaft by deep dorsal and lateral depressions. The distal articulation is epiphyseal and symmetrical, with the inner tuberosity larger than the external one. On the palmar or inferior surface, they develop a short ridge in the median line. In general, the distal articulation is almost straight on the inner side and strongly curved on the external side. The articular surface of the proximal epiphysis forms almost a right angle to the beginning of the shaft, and the dorsal surface widens much more posteriorly. On the inside of the shaft is an oval, wide articular surface that joins the protruding part of mc 2. These two articular surfaces are separated from each other by a well-marked ridge. On the outside are two concave surfaces for contact with mc 4. They are not as strongly concave and are more strongly connected than those for contact with mc 2. The distal epiphysis is elliptical and symmetrical.

Metacarpal 5 (mc 5). The mc 5 is the largest and the most massive among all metapodials (Fig. 8D). Its proximal epiphysis is strongly thickened and flattened. The proximal articulation for the hamatum forms a continuous surface with that of mc 4, as it is convex only in vertical direction and covers the entire end of the bone. The intermetacarpal articulation is flattened, segmental in form, set at right angles to that for the hamatum. In front, there rises an articular surface, which fits into a corresponding hollow in mc 4. Both proximal articulation facets run gently from mesial to distal and protract medially. The medial articulation surface (for mc 4) shows two round areas. The larger, mesial area, runs down distally into a triangular area. Externally, its head presents a large tuberosity, which affords attachment to strong ligaments that bind the bone to the hamatum, cuneiform, and pisiform. In addition, there is a large tuberosity on the palmar surface. The proximal epiphysis is deeply convex and the mesial limit ends with an acute angle. Laterally, it develops a bulge and forms a semilunar convex sur-

face. The shaft is proportionally shorter and more robust than triangular in section, to be more tapering, and to arch more decidedly in a palmar and outward direction than any other metacarpal bone. The distal epiphysis is strongly convex externally and concave internally, and the outer tuberosity is larger and set lower on the bone than the inner one. The medial part is narrower, while the palmar process is large and well-developed.

The proximal articular surface of mc 5 is much less concave than those in mtcp 2 and 3. The structure of mc 5 is much more massive than that of the other metacarpals, and the curvature of the dorsal surface is more flattened. The proximal metacarpal is very massive and flattened. The articular surface of the proximal epiphysis for contact with the hamate forms a continuous surface with that for contact with mc 4. It is convex only in the vertical direction and covers almost the entire surface of the bone. The inner surface for contact with the other metacarpals has a flattened surface, is set perpendicular to the articular surface for contact with the hamate and is interrupted in the lower part by large notches for ligaments. Opposite is a convex articular surface, which fits into a corresponding depression in mc 4. Both articular surfaces for metacarpals 4–5 pass gently from front to back. Externally, the proximal epiphysis presents a large, strongly tuberous articular surface, the site of attachment of strong ligaments that connected mc 5 to the cuneiform, hamate, and pisiform bones. There is also a large tuberosity on the palmar surface. The proximal epiphysis is strongly convex and the anterior edge ends in a sharp angle. Transversely, it has a strong bulge and forms a semilunar, convex surface. The shaft is proportionally shorter and more massive than in other metacarpals (Fig. 8D). It is also simultaneously more strongly arched outwards. The proportionally slender distal epiphysis is strongly convex outwards and concave inwards (Fig. 8D). The external tuberosity is larger and set lower than the internal one. This structure is divided into two parts of unequal size by a transverse crest. The medial part is narrower, while the palmar process is large and well-developed.

Metatarsal 1 (mt 1). The proximal articulation of mt 1 is formed by a medial concavity that is frontally bulged and distally directed to the medial side (Fig. 8E, F). It also narrows pointedly in its distal direction, and has a triangular shape. Laterally, there are two well-marked surfaces, both concave and joined to mt 3. The proximal articular surface for the entocuneiform is well pronounced and its median ridge is strongly shifted dorsally, while it is enlarged and curved frontally. Medially, it forms a short constriction and a distal bulge. The articular surfaces for mt 3 are separated from each other, the distal one being much larger and rounded. The proximal articulation facet for tarsal 2 is composed of two different areas, clearly separated by large, well-developed, rounded and differently sized incisions. The mesial part is strongly widened and curved, triangular in shape. The distal part is smaller and rectangular in shape. An elongated, smaller indentation, shifted towards the medial side, is positioned centrally. The larger indentation is more oval-shaped, situated more laterally and runs mesio-medially. Medially, the articular surface is divided into two sides: frontally, the first one is horizontally elongated, stretching out and sloping to the medial plane. Behind, there is a flat and short end of the surface. Frontally, there is one concavity, similar to that described on the previous bone. The medial articulation is divided into two parts, a smaller mesial and larger distal one. Both areas are separated by a semi-circular incision, strongly pleated at the base. The lateral indentation is similarly developed and also splits into two, dimensionally different areas. The medial crest and a medial articulation facet slope towards the medial side and are quite shallow and elongated (Fig. 8E, F).

The quadrate proximal epiphysis has a large, shallow and almost smooth articular surface. The shaft is proportionally narrow and curved, with a rounded cross-section (Fig. 8E, F). Frontally, there is a small bulge and depressions on the medial surface. It ends in front of a distal convexity. In lateral view, just next to the base, there is an elongated articular surface, the site of attachment of mt 2. Above this concavity, on the anterolateral corner, there is a horizontal convexity. The trochlea is well-developed and narrow, with a more pronounced medial crest running along its plantar side than in *U. a. arctos* (Fig. 8E, F).

Metatarsal 2 (mt 2). The mt 2 has a massive and curved diaphysis, front-distally flattened and rectangular (Fig. 8J). The distal articulation is relatively large, rounded, and irregular. The medial epicondyle is more prominent than the lateral one. The articular surface of the proximal epiphysis for contact with mt 3 is smaller anteriorly and tilts slightly anteriorly. The lateral and medial articular surfaces of the proximal epiphysis differ from those of *U. a. arctos* individuals. This part of mt 2 is more massive and lacks the deep notch on the dorsal surface. The body shows a noticeable dorso-ventral flattening, and the medial part of the ridge of the proximal epiphysis is less curved than in *U. a. arctos*. The articular surface proximal to the body is formed by a medial concavity that bulges antero-posteriorly. It also tapers significantly posteriorly and has a triangular shape. Laterally located are two well-developed articular surfaces, both concave, for articulation with mt 3. The articular surface of the distal epiphysis is relatively large and rounded. All features show a clear similarity to *U. a. arctos*, but differ in a straighter articular surface. In general, the articular surfaces are more massive in fossil brown bears. In summary, it can be said that the most noticeable differences between fossil and modern brown bears among all metatarsal bones are noticeable in mt 2 (Fig. 8J).

Metatarsal 3 (mt 3). This bone is characterised by a massive and curved shaft, flattened in the antero-posterior direction. The massiveness indices are proportionally among the highest for all metacarpals and metatarsals (Fig. 8G, H). The articular surface for the mesocuneiform is well developed, and its medial ridge is strongly shifted outwards. Medially, it forms a short narrowing. The articular surfaces for mt 4 are separated far from each other, and the posterior one is much larger and rounded. The proximal articular surface for contact with the ectocuneiform consists of two distinct surfaces, clearly separated from each other by large notches. The anterior part is expanded, in the shape of an unequal-sided triangle, and strongly curved. The posterior part is smaller, rectangular in shape. The elongated, smaller notch is shifted towards the medial wall and is located centrally. The larger notch is more oval, located more laterally and further anteromedially. Medially, the articular surface is divided into two parts: from the front, the first is stretched horizontally. The second, posterior, is flat and shorter. The medial articular surface is divided into two parts, a smaller anterior and a larger posterior part. Both areas are separated from each other by a semicircular notch. The lateral articular surface is similarly developed, and is divided into two, also dimensionally different areas. The medial crest and the medial articular surface are moderately shallow and elongated. The width of the shaft increases slightly from the proximal to the distal epiphysis. In lateral view, just below the proximal epiphysis, there is a protrusion of the shaft. The distal epiphysis has a regular shape, almost equally curved on both sides. The medial condyle is only slightly more developed than the lateral condyle (Fig. 8G, H).

The diaphyseal depth of mt 3 barely declines from proximal to distal (Fig. 8G, H). Two large rounded indentations of different size are notable on the proximal articulation facet for the ectocuneiform. The latter is composed of a distal, approxi-

mately rectangular part and another part, widening towards mesial, which has the shape of a non-isosceles triangle, the curved basis of which points mesially. Both parts are clearly separated in the assumed overlapping area by two incisions spanning from medial to lateral. The medial articulation facet is split into two parts. It is developed into a smaller mesial and a larger distal partial facet, which are separated by an incision that ends distally in a semi-circular shape, the base of which is strongly pleated.

Metatarsal 4 (mt 4). The outline of the proximal articulation facet of mt 4 corresponds to that of *U. a. arctos*, only the mesio-medial articulation facet is more prominent and rectangularly shaped (Fig. 8I, J). The diaphysis is slightly more elongated and built more stoutly. In frontal view, the diaphysis widens strongly towards the proximal epiphysis. Its holds a medial crista and a medial articulation facet which slopes towards the medial side. The lateral epicondyle is more prominent than the medial epicondyle.

Compared to other metatarsals, mt 4 is more massive, with a thicker and less curved shaft (Fig. 8I, J). The articular surface for contact with the cuboid bone is convex, slightly higher at the distal edge, and frontally inclined. The lateral surface of the proximal epiphysis is rectangular, and behind it there is a deep convexity. The articular surface is inclined and convex, rectangular, ending in the front in the form of a curved, large edge. On the plantar side, the proximal articular surface ends in a horizontal pattern. This part is elongated, separated from the posterior part by a shallow notch. At the contact with mt 3 there is an inclined, slightly curved, elongated surface. The massive and almost straight shaft in the lateral projection is slightly curved. Above the distal epiphysis there is a large tuberosity on both sides of the shaft at the radial attachment of the flexors (Fig. 8I, J).

Metatarsal 5 (mt 5). This is the longest and proportionally the most slender of all the metatarsals (Fig. 8K, L). The proximal epiphysis is shaped like an irregular umbrella, with two lobes. The articular surface of these two lobes is tilted medially. The contact point with mt 4 is formed by an enlarged frontal surface. The shaft is triangular in cross-section and almost straight. It narrows slightly towards the distal metacarpal, and its narrowest point is located at about two-thirds of its length. The medial thickening, located on the plantar side of the shaft, is poorly developed. The distal epiphysis is regularly built. The medial protuberance of mt 5 is moderately developed on the plantar side of the diaphysis. It widens continually to merge with the distal articulation. The diaphysis tapers off distally, and its narrowest point is within the proximal third of the diaphysis. The medio-plantar protuberance in the area of the distal diaphysis is somewhat more strongly developed.

The length of all metapodials from JN exceed the length of those of *U. s. ingressus*. Only the smallest of them are comparable in length with the largest specimens of *U. s. ingressus* (Fig. 8K, L). All indices are significantly below those typical of *U. s. ingressus*. In general, metapodials of *U. a. taubachensis* and *U. a. arctos* are longer and more slender, and the articular surfaces are less developed and usually more convex than those in *U. s. ingressus*. Metapodials of *U. a. taubachensis* are larger and distinctly more robust than those of *U. a. arctos* (Tables 2 and 3). The shaft is not as straight and the articular surfaces are more strongly developed. Analysis of metapodials from JN fully confirmed the determination of the material as that belonging mostly to *U. a. taubachensis* and in a few specimens to *U. a. arctos*. No substantial differences between JN material and those from other Late Pleistocene populations were found. Their dimensions, K-index and P-index are variable, but generally fall within the size variability of equal bones (Tables 2 and 3).

DISCUSSION

The material of *U. arctos* from JN is represented by material of great taxonomic value. The specific cranial and dental characteristics of many Late Pleistocene populations of *U. arctos*, especially from periglacial areas, cannot be disputed. They are commonly represented in France and the Netherlands through Central and East Europe to North Siberia and Yakutia (Erdbrink, 1953, 1969; Mostecky, 1963; Musil, 1964; Ballesio, 1983; Baryshnikov and Boeskorov, 2004; Marciszak et al., 2019, 2020, 2021, 2024a). Those bears from the late Middle and Late Pleistocene (MIS 12-2) were characterised by a unique combination of features, unknown in extant representatives of *U. arctos*. The problem is that, with the exception of some Eemian sites (e.g., Taubach in Germany, Dziadowa Skała in Poland and Chlupáčova sluj in Czech Republic), the Late Pleistocene records of *U. arctos* are rather fragmentary, not allowing sufficient characterisation of population variability. We therefore decided to leave the question of taxonomic status of Late Pleistocene bears open. The term *U. a. taubachensis* is used for a large form corresponding to the traditional concept of "*U. a. priscus*" (leaving aside the fact that these phenotypic characteristics do not fit to the holotype of *U. a. priscus* itself). *U. a. arctos* is restricted the European Holocene brown bear, identical to the extant, nominotypical subspecies *U. a. arctos* (Marciszak et al., 2022).

With the material of *U. arctos* from JN we are certainly dealing with two subspecies living in different periods and climatic and palaeoenvironmental conditions. The overwhelming majority of the material of this species comes from the Late Pleistocene (MIS 3-2), and belongs to *U. a. taubachensis*. This bear is regarded as an inhabitant of extensive open grasslands and lowlands, which regularly also visited mountains like the Sudetes, mainly in search of food (Sabol, 2001; Barysnikov, 2007; Marciszak et al., 2020, 2024b).

The analysis of mitochondrial ancient DNA (aDNA) shows a high Late Pleistocene diversity across the continent and challenges somehow the idea of strict confinement to traditional southern refugia during the last glacial maximum (LGM) (Ersmark et al., 2019). The mitochondrial data suggest a genetic turnover just before the LGM. Analysis of a few specimens from JN confirmed their attribution to *U. arctos* and to the subclade 1b, the same as in the extant nominotypical subspecies *U. a. arctos* from the Carpathian Mts. These results were also obtained for specimens which morphologically were assigned to *U. a. arctos*, while in those determined as *U. a. taubachensis* so far no DNA has been found (Ersmark et al., 2019). In subclade 1b, the most intensive dynamics start around 17–16 ka. After this point, 1b was widespread across central Europe and was present also in Denmark and in southeastern France. Today, this haplotype is also by far the most widespread in Central Europe. However, despite the extensive spread of subclade 1b in Western Europe it was preceded by subclade 1a. There are also no traces of 1b expanding into the Iberian Peninsula, the British Isles or Scandinavia (Ersmark et al., 2019).

The material of Niedźwiedzia Cave clearly documents a decrease in size, and morphological changes in, the evolutionary lineage of this species (Fig. 9). *U. a. taubachensis* roamed on Eurasian Late Pleistocene open grasslands and penetrated mountain areas in seach of food (Baryshnikov and Boeskorov, 2005; Marciszak et al., 2019). The European pre-LGM brown bears, compared with the extant *U. arctos*, were distinctly more carnivorous, as was inferred from stable isotope analyses (Münzel et al., 2011; Bocherens, 2015; Bocherens et al., 2015; Ersmark et al., 2019). This also suggests that the shift to lower

Fig. 9. Comparison of the size of two brown bear subspecies from Niedźwiedzia Cave with a man 180 cm tall

On the left *Ursus arctos arctos* (MIS 1), on the right *Ursus arctos taubachensis* (MIS 3). Drawing by W. Gornig

^{15}N values started after the LGM and was synchronous with the extinction of *U. spelaeus* sensu lato. This dietary shift reflects the opening of a more herbivorous niche for *U. arctos* (Münzel et al., 2011; Bocherens, 2015; Mackiewicz et al., 2017). However, higher ^{15}N values in the Late Pleistocene *U. arctos* from MIS 3-2 could have been an adaptation to colder and more barren habitats. Recent brown bears are generally more carnivorous in open landscapes (Bojarska and Selva, 2012; Ersmark et al., 2019). Some earlier authors pointed out that the presence of *U. a. taubachensis* was characteristic of open and periglacial grasslands (Thenius,1956; Musil, 1964). This period is documented by most of the material dated to MIS 3-2, robust and giant individuals, which probably penetrated the Niedźwiedzia Cave in search of food, and maybe also as hibernating cave bears (Marciszak et al., 2024b).

An abrupt warming at 14.7 ka (onset of GI-1e), and a reduction and fragmentation of the *U. a. taubachensis* range, are suggested for a wide area of Europe. This was except in more oceanic north-western parts, such as the modern Baltic and North Sea coasts and perhaps the central and northern East European Plain. A possible explanation for the longer survival of *U. a. taubachensis* is that the steppe-tundra ecosystem in these regions lasted longer (Coles, 2000). Between 15–13.5 ka, the present-day Baltic and North Sea coasts, as well as the north-western part of Europe, were still covered by open grassland vegetation suitable for *U. a. taubachensis*, in contrast to Central Europe, which was already covered by pine forests (Brewer et al., 2017). This turnover is corroborated by the presence of *U. a. arctos* remains, dated to 14.0–13.6 cal ka BP, morphologically indistinguishable from the extant Carpathian population.

Funding

The research was financed by an internal grant from the Faculty of Biological Sciences, University of Wrocław entitled "The Middle Pleistocene Revolution – how the modern theriofauna of Eurasia was developed", as part of the programme "Inicjatywa Doskonałości – Uczelnia Badawcza (IDUB)", grant no. BPIDUB.4610.6.2021.KP.A.

Data availability statement

All information where readers can obtain the research data required to reproduce the work reported in the manuscript, e.g. status of the material, its location, collection numbers etc., are

provided within the manuscript and in both appendices. All material, if currently present, is available to study at the Department of Palaeozoology, University of Wrocław.

Conflict of interest

The authors declare no conflicts of interest. The funders had no role in the design of the study, in the collection, analysis, or interpretation of data, in the writing of the manuscript, or in the decision to publish the results.

Acknowledgments. We are indebted to two reviewers, Bogdan Ridush and Tomáš Čeklovský, for their useful comments and suggestions, which made meaningful improvements to the original manuscript.

REFERENCES

Baca, M., Stankovic, A., Stefaniak, K., Marciszak, A., Hofreiter, M., Nadachowski, A., Węgleński, P., Mackiewicz, P., 2012. Genetic analysis of cave bear specimens from Niedźwiedzia Cave, Sudetes, Poland. Palaeontologia Electronica, **15**: 1–16; https://doi.org/10.26879/301

Baca, M., Mackiewicz, P., Stankovic, A., Popović, D., Stefaniak, K., Czarnogórska, K., Nadachowski, A., Gąsiorowski, M., Hercman, H., Węgleński, P., 2014. Ancient DNA and dating of cave bear remains from Niedźwiedzia Cave suggest early appearance of *Ursus ingressus* in Sudetes. Quaternary International, **339–340**: 217–223; https://doi.org/10.1016/j.quaint.2013.08.033

Ballesio, R., 1983. Le gisement Pléistocène supérieur de la grotte de Jaurens á Nespouls, Corrèze, France: les Carnivores (Mammalia, Carnivora). III. Ursidae - *Ursus arctos* Linnaeus. Archives du Muséum d'histoire naturelle de Lyon, **21**: 9–43.

Baryshnikov, G.F., 2007. Semeistvo medvezhiye (Carnivora, Ursidae) (in Russian). Nauka, Sankt-Peterburg.

Baryshnikov, G.F., Boeskorov, G.G., 2004. Skull of the Pleistocene brown bear (*Ursus arctos*) from Yakutia, Russia. Russian Journal of Theriology, **3**: 71–75; https://doi.org/10.15298/rusjtheriol.3.2.04

Bocherens, H., 2015. Isotopic tracking of large carnivore palaeoecology in the mammoth steppe. Quaternary Science Reviews, **117**: 42–71; https://doi.org/10.1016/j.quascirev.2015.03.018

Bocherens, H., Drucker, D.G., Germonpré, M., Láznič-ková-Galetová, M., Naito, Y.I., Wissing, Ch., Brůžek, J., Oliva, M., 2015. Reconstruction of the Gravettian food-web at Předmostí I using multi-isotopic tracking (^{13}C, ^{15}N, ^{34}S) of bone collagen. Quaternary International, **359–360**: 211–228; https://doi.org/10.1016/j.quaint.2014.09.044

Bojarska, K., Selva, N., 2012. Spatial patterns in brown bear *Ursus arctos* diet: the role of geographical and environmental factors. Mammal Review, **42**: 120–143; https://doi.org/10.1111/j.1365-2907.2011.00192.x

Bonifay, M.F., 1966. Les carnivores: Canidés, Hyaenidés, Felidés et Mustelidés. In: Atlas de Préhistoire. Tome III. Faunes et flores préhistoriques de l'Europe occidental (eds. R. Lavocat and J. Piveteau): 337–396. L'homme et ses origins, Paris.

Brewer, S., Giesecke, T., Davis, B.A., Finsinger, W., Wolters, S., Binney, H., de Beaulieu, J.-L., Fyfe, R., Gil-Romera, G., Kühl, N., Kuneš, P., Leydet, M., Bradshaw, R.H., 2017. Late glacial and Holocene European pollen data. Journey Maps, **13**: 921–928; https://doi.org/10.1080/17445647.2016.1197613

Coles, B.J., 2000. Doggerland: the cultural dynamics of shifting coastline. Geological Society Special Publications, **175**: 393–401; https://doi.org/10.1144/GSL.SP.2000.175.01.2

Davison, J., Ho, S.Y.W., Bray, S.C., Korsten, M., Tammeleht, E., Hindrikson, M., Østbye, K., Østbye, E., Lauritzen, S.-E., Austin, J., Cooper, A., Saarma, U., 2011. Late-Quaternary biogeographic scenarios for the brown bear (*Ursus arctos*), a wild mammal model species. Quaternary Science Reviews, **30**: 418–430; https://doi.org/10.1016/j.quascirev.2010.11.023

Edwards, C.J., Ho, S.Y.W., Barnett, R., Coxon, P., Bradley, D.G., Lord, T.C., O'Connor, T., 2014. Continuity of brown bear maternal lineages in northern England through the Last-glacial period. Quaternary Science Reviews, **96**: 131–139; https://doi.org/10.1016/j.quascirev.2013.10.015

Ehrenberg, K., 1938. Über einige weitere Ergebnisse der Untersuchungen an den Bären von Winden. Verhandlungen der Zoologisch-Botanischen Gesellschaft in Wien, **86–87**: 388–395.

Erdbrink, D.P., 1953. A review of fossil and recent bears of the Old World, with remarks on their phylogeny, based upon their dentition. Jan de Lange, Deventer.

Erdbrink, D.P., 1967. New finds of fossil bears from The Netherlands. Lutra, **9**: 17–41.

Ersmark, E., 2016. Large carnivore population turnover and ecological change during the Late Quaternary. Ph.D. thesis. Department of Zoology, Stockholm University.

Ersmark, E., Baryshnikov, B., Higham, T., Argant, A., Castaños, P., Döppes, D., Gasparik, M., Germonpré, M., Lidén, K., Lipecki, G., Marciszak, A., Miller, R., Moreno García, M., Pacher, M., Robu, M., Rodriguez Varela, R., Rojo Guerra, M., Sabol, M., Spassov, N., Storå, J., Valdiosera, Ch., Villaluenga, A., Stewart, J.R., Dalén, L., 2019. Genetic turnovers and northern survival during the last glacial maximum in European brown bears. Ecology and Evolution, **9**: 5891–5905; https://doi.org/10.1002/ece3.5172

Goldfuss, A., 1818a. Beschreibung eines fossilen Vielfrass-Schädels aus der Gailenreuther Höhle. Nova Acta Physico-Medica Academiae Caesareae Leopoldino-Carolinae, **9**: 313–322.

Goldfuss, A., 1818b. Descriptio cranii ex ursorum genere memorabilis, nuperrime in cavernis prope Muggendorf reperti. Nova Acta Physico-Medica Academiae Caesareae Leopoldino-Carolinae, **10**: 259–276.

Gunther, R.T., 1923. *Ursus anglicus*, a new species of British bear. The Annals and Magazine of Natural History, **11**: 490–496.

Haroldson, M.A., Clapham, M., Costello, C.C., Gunther, K.A., Kendall, K.C., Miller, S.D., Pigeon, K.E., Proctor, M.F., Rode, K.D., Servheen, Ch., Stenhouse, G., van Manen, F.T., 2020. Brown bear (*Ursus arctos*, North America). In: Bears of the World. Ecology, Conservation and Management (eds. V. Penteriani and M. Melletti): 162–195. Cambridge University Press, Cambridge, Great Britain.

Ingólfsson, Ó., Wiig, Ø., 2008. Late Pleistocene fossil find in Svalbard: the oldest remains of a polar bear *(Ursus maritimus* Phipps, 1744) ever discovered. Polar Research, **28**: 455–466; https://doi.org/10.1111/j.1751-8369.2008.00087.x

Jakubiec, Z., 1993. *Ursus arctos* Linnaeus, 1758 – Braunbär. In Handbuch der Säugetiere Europas, Raubsäuger – Carnivora (Fissipedia). Teil I: Mustelidae 2, Viverridae, Herpestidae, Felidae, **5** (eds J. Niethammer and F. Krapp): 254–300. AULA Verlag, Wiesbaden.

Jánossy, D., 1963. Letzinterglaziale Vertebratenfauna aus der Kalman Lambrecht Höhle (Bükk-Gebirge, Nordost Ungarn). Teil I. Acta Zoologica Academiae Scientiarum Hungaricae, **9**: 139–197.

Kosintsev, P.A., Bocherens, H., Kirillova, I.V., Levchenko, V.A., Zazovskaya, E.P., Trofimova, S.S., Lan, T., Lindqvist, C., 2022. Palaeoecological and genetic analyses of Late Pleistocene bears in Asiatic Russia. Boreas, **51**: 465–480; https://doi.org/10.1111/bor.12570

Kurtén, B., 1956. The bears and hyenas of the interglacials. Quaternaria, **4**: 1–13.

Kurtén, B., 1959. On the bears of the Holsteinian Interglacial. Stockholm Contribution in Geology, **2**: 73–102.

Kurtén, B., 1964. The evolution of the polar bear, *Ursus maritimus* Phipps. Acta Zoologica Fennica, **108**: 1–26.

Mackiewicz, P., Baca, M., Popović, D., Socha, P., Stefaniak, K., Marciszak, A., Nadachowski, A., 2017. Estimating the extinction time of two cave bears, *Ursus spelaeus* and *U. ingressus*. Acta Zoologica Cracoviensia, **60**: 1–14; https://doi.org/10.3409/azc.60_2.01

Marciszak, A., Stefaniak, K., Mackiewicz, P., Ridush, B., 2015. *Ursus arctos* L., 1758 from Bukovynka Cave (W Ukraine) in an overview on the fossil brown bears size variability based on cranial material. Quaternary International, **357**: 136–148; https://doi.org/10.1016/j.quaint.2014.09.052

Marciszak, A., Schouwenburg, C., Lipecki, G., Talamo, S., Shpansky, A., Malikov, D., Gornig, W., 2019. Steppe brown bear *Ursus arctos* "*priscus*" from the Late Pleistocene of Europe. Quaternary International, **534**: 158–170; https://doi.org/10.1016/j.quaint.2019.02.042

Marciszak, A., Sobczyk, A., Kasprzak, M., Gornig, W., Ratajczak, U., Wiśniewski, A., Stefaniak, K., 2020. Taphonomic and paleoecological aspects of large mammals from Sudety Mts (Silesia, SW Poland), with particular interest to the carnivores. Quaternary International, **546**: 42–63; https://doi.org/10.1016/j.quaint.2019.11.009

Marciszak, A., Wagner, J., Kyselý, R., Matyaszczyk, L., Roblíčková, M., Plichta, A., Káňa, V., 2022. The Late Pleistocene history of the brown bear *Ursus arctos* Linnaeus, 1758 in the Czech Republic. Radiocarbon, **64**: 1483–1499; https://doi.org/10.1017/RDC.2022.65

Marciszak, A., Kropczyk, A., Demidziuk, K., Gornig, W., Nowakowski, D., 2024a. Mammal record and Palaeolithic bear cult in Europe: a review from Radochowska Cave (Sudety Mts, SW Poland). Historical Biology, **36**: 689–718; https://doi.org/10.1080/08912963.2023.2180743

Marciszak, A., Mackiewicz, P., Borówka, R.K., Capalbo, C., Chibowski, P., Gąsiorowski, M., Hercman, H., Cedro, B., Kropczyk, A., Gornig, W., Moska, P., Nowakowski, D., Ratajczak-Skrzatek, U., Sobczyk, A., Sykut, M.T., Zarzecka-Szubińska, K., Kovalchuk, O., Barkaszi, Z., Stefaniak, K., Mazza, P.P.A., 2024b. Fate and preservation of the Late Pleistocene cave bears from Niedźwiedzia Cave in Poland, through taphonomy, pathology, and geochemistry. Scientific Reports, **14**, 9775; https://doi.org/10.1038/s41598-024-60222-3

Mostecký, V., 1963. Der pleistozäne Bär *Ursus taubachensis* Rode aus der Schlucht "Chlupáčova Sluj" bei Koněprusy (Mittelböhmen, unweit Beroun). Acta Musei Nationalis Pragae, Series B – Historia Naturalis, **19**: 75–101.

Mostecký, V., 1969. Jungpleiztozäne Säugethiere aus der "Chlupáč-Höhle" auf dem Hügel "Kobyla" bei Koněprusy (Böhmischer Karst). Acta Musei Nationalis Pragae, Series B – Historia Naturalis, **25B**: 1–28.

Münzel, S.C., Stiller, M., Hofreiter, M., Mittnik, A., Conard, N.J., Bocherens, H., 2011. Pleistocene bears in the Swabian Jura (Germany): genetic replacement, ecological displacement, extinctions and survival. Quaternary International, **245**: 225–237; https://doi.org/10.1016/j.quaint.2011.03.060

Musil, R., 1964. Die Braunbären aus dem Ende des lezten Glazials. Časopis Moravského Musea v Brně, **49**: 83–102.

Pacher, M., 2007. The type specimen of *Ursus priscus* Goldfuss, 1810 and the uncertain status of Late Pleistocene brown bears. Neues Jahrbuch für Geologie und Paläontologie Abhandlungen, **245**: 331–339; https://doi.org/10.1127/0077-7749/2007/0245-0331

Pacher, M., 2017. Anterior premolar variability in Pleistocene cave and brown bears and its significance in species determination. Fossil Imprint, **73**: 482–494; https://doi.org/10.1515/if-2017-0025

Petronio, C., Canzio, E.d., Stefano, G.D., 2003. Morphological and biometrical differences in the limb bones of *Ursus arctos* and *Ursus spelaeus* and phylogenetical consideraqtions of the two species. Palaeontographica A, **269**: 137–152; https://doi.org/10.1127/pala/269/2003/137

Rabeder, G., 1983. Neues vom Höhlenbären: zur Morphogenetik der Backenzähne. Die Höhle, **34**: 67–85.

Rabeder, G., 1995. Die Gamssulzenhöhle im Toten Gebirge. Mitteilungen der Kommission für Quartärforschung der Österreichischen Akademie der Wissenschaften, **9**: 1–133.

Rabeder, G., 1999. Die Evolution des Höhlenbärengebisses. Mitteilungen der Kommission für Quartärforschung der Österreichischen Akademie der Wissenschaften, **11**: 1–102.

Rabeder, G, Pacher, M, Withalm, G., 2010. Early Pleistocene bear remains from Deutsch-Altenburg (Lower Austria). Mitteilungen der Kommission für Quartärforschung der Österreichischen Akademie der Wissenschaften, **17**: 1–135.

Sabol, M., 2001. Fossil and subfossil findings of brown bears from selected localities in Slovakia. Slovak Geological Magazine, **7**: 3–17.

Sobczyk, A., Kasprzak, M., Marciszak, A., Stefaniak, K., 2016. Karst phenomena in metamorphic rocks in the Śnieżnik Massif (Eastern Sudetes): current state of research and significance for understanding the evolution of the Sudetes in the late Cenozoic (in Polish with English summary). Przegląd Geologiczny, **64**: 710–718.

Swenson, J.E., Ambarlý, H., Arnemo, J.M., Baskin, L., Ciucci, P., Danilov, P.I., Delibes, M., Elfström, M., Evans, A.L., Groff, C., Hertel, A.G., Huber, D., Jerina, K., Karamanlidis, A.A., Kindberg, J., Kojola, I., Krofel, M., Kusak, J., Mano, T., Melletti, M., Mertzanis, Y., Ordiz, A., Palazón, S., Parchizadeh, J., Penteriani, V., Quenette, P.-Y., Sergiel, A., Selva, N., Seryodkin, I., Skuban, M., Steyaert, S.M.J.G., Střen, O.-G., Tirronen, K.F., Zedrosser, A., 2020. Brown bear (*Ursus arctos*, Eurasia). In: Bears of the World. Ecology, Conservation and Management (eds. V. Penteriani and M. Melletti): 139–161. Cambridge University Press, Cambridge.

Sommer, R.S., Benecke, N. 2005. The recolonization of Europe by brown bears *Ursus arctos* Linnaeus, 1758 after the Last Glacial Maximum. Mammal Review, **35**: 156–164; https://doi.org/10.1111/j.1365-2907.2005.00063.x

Thenius, E., 1956. Zur Kenntnis der fossilen Braunbären (Ursidae, Mammalia). Sitzungsberichte der Kaiserlichen Akademie der Wissenschaften. Mathematisch-Naturwissenschaftliche Klasse, **165**: 153–172.

Valdiosera, C.E., Garcia-Garitagoitia, J.L., Garcia, N., Doadrio, I., Thomas, M.G., Hänni, C., Arsuaga, J.L., Barnes, I., Hofreiter, M., Orlando, L., Götherström, A., 2008. Surprising migration and population size dynamics in ancient Iberian brown bears (*Ursus arctos*). Proceedings of the National Academy of Sciences of the United States of America, **105**: 5123–5128; https://doi.org/10.1073/pnas.0712223105

Torres Pérez Hidalgo, T.de., 1988. Osos (Mammalia, Carnivora, Ursidae) del Pleistoceno Ibérico (*U. deningeri* Von Reichenau, *U. spelaeus* Rosenmüller-Heinroth, *U. arctos* Linneo): V. Dentición decidual, fórmula dentaria y dentición superior. Boletin Geológico y Minero, **99**: 660–714.

Wiszniowska, T., 1967. A new paleontological find in the Sudetes (in Polish with English summary). Przegląd Zoologiczny, **11**: 430–433.

Wiszniowska, T., 1970. Preliminary results of fossil fauna research in the Niedźwiedzia Cave (in Polish with English summary). Acta Universitatis Wratislaviensis, **127**: 45–70.

Wiszniowska, T., 1976. The cave bear from Kletno and other caves in Poland (in Polish with English summary). Acta Universitatis Wratislaviensis, **311**: 1–75.

Wiszniowska, T., 1978. *Panthera spelaea* (Goldfuss) from Niedźwiedzia Cave in Kletno (in Polish with English summary). Acta Universitatis Wratislaviensis, **329**: 113–141.

Wiszniowska, T., 1986. Remains of fauna in the silts of caves in Silesia (in Polish with English summary). Prace Komisji Archeologicznej Polska Akademia Nauk Ossolineum, **3**: 9–19.

Wiszniowska, T., 1989. Kopalne szczątki zwierzęce (in Polish) In: Jaskinia Niedźwiedzia w Kletnie. Badania i udostępnianie (eds. A. Jahn, S. Kozłowski and T. Wiszniowska): 255–279. Zakład Narodowy Imienia Ossolińskich, Wrocław-Warszawa.

Withalm, G., 2001. Die Evolution der Metapodien in der Höhlenbären-Gruppe (Ursidae, Mammalia). Beiträge zur Paläontologie, **26**: 169–249.

APPENDIX 1

Cataloque no.	Description	Subspecies	Trench	Layer	Old catalogue no.	Depth	Year
JN.5.1	left mandible with damaged ramus, p1 and	*Ursus arctos taubachensis*	K II	21	K 527		
JN.5.2	right mandible with p4 and m2	*Ursus arctos arctos*	K V	12			
JN.5.3	body of the right mandible with worn m2	*Ursus arctos taubachensis*	K I	13			
JN.5.4	mesial part of the right mandible with c1	*Ursus arctos taubachensis*	K II	7			
JN.5.5	right radius	*Ursus arctos arctos*	K I	5			
JN.5.6	right ulna	*Ursus arctos arctos*	K II	18	K 154		
JN.5.7	distal epiphysis with shaft fragment of righ	*Ursus arctos taubachensis*	K V	23	K 256/78		
JN.5.8	right talus	*Ursus arctos taubachensis*	K II	17	K 300		
JN.5.9	left talus	*Ursus arctos taubachensis*	K IV	14	K 392/78		
JN.5.10	left calcaneus	*Ursus arctos taubachensis*	K V	23	K 5/67		
JN.5.11	right calcaneus	*Ursus arctos taubachensis*	K V	21	K 5/40		
JN.5.12	right metatarsal 4	*Ursus arctos taubachensis*	K II	18	K 68/77		
JN.5.13	right metacarpal 5	*Ursus arctos taubachensis*	K V	16			
JN.5.14	left metatarsal 4	*Ursus arctos taubachensis*	K V	21	K-5-X		
JN.5.15	right metacarpal 2	*Ursus arctos taubachensis*	K IV	15			
JN.5.16	right metatarsal 5	*Ursus arctos taubachensis*	K IV	16			
JN.5.17	left metatarsal 5	*Ursus arctos taubachensis*	K II	17	K 902		
JN.5.18	right metatarsal 5	*Ursus arctos taubachensis*	K III	13			
JN.5.19	left metatarsal 5	*Ursus arctos taubachensis*	K V	20	K-5-X		
JN.5.20	left metatarsal 1	*Ursus arctos taubachensis*	K V	22	K-5-X		
JN.5.21	right metatarsal 1	*Ursus arctos taubachensis*	K V	24	K 5/86		
JN.5.22	right metacarpal 1	*Ursus arctos arctos*	K II	18	K 163		
JN.5.23	left metacarpal 1	*Ursus arctos taubachensis*	K IV	12	K 593/78		
JN.5.24	right metatarsal 5	*Ursus arctos taubachensis*	K V	19	K 5/50		
JN.5.25	left metatarsal 5 without distal epiphysis	*Ursus arctos taubachensis*	K VI	20	KH/10-91	115-130	1991
JN.5.26	right metacarpal 5	*Ursus arctos taubachensis*	K V	23	K-5-X		
JN.5.27	right metatarsal 3	*Ursus arctos taubachensis*	KCP		K 1378/93	120-130	1993
JN.5.28	left metatarsal 2	*Ursus arctos taubachensis*	K V	23	K-5-X		
JN.5.29	right metatarsal 3	*Ursus arctos taubachensis*	K IV	24			
JN.5.30	left metatarsal 3	*Ursus arctos taubachensis*	K IV	17	K 690		
JN.5.31	right metatarsal 3	*Ursus arctos taubachensis*	K V	22	K 5/70		
JN.5.32	left metatarsal 3	*Ursus arctos taubachensis*	K V	19	K-5-X		
JN.5.33	right metacarpal 3	*Ursus arctos taubachensis*	K I	4			
JN.5.34	right metacarpal 3	*Ursus arctos taubachensis*	K V	16			
JN.5.35	left metatarsal 4	*Ursus arctos taubachensis*	K V	23	K 5/59		
JN.5.36	right metatarsal 4	*Ursus arctos taubachensis*	K II	17			
JN.5.37	phalanx 1	*Ursus arctos taubachensis*	K V	23			
JN.5.38	phalanx 1	*Ursus arctos taubachensis*	K V	23			
JN.5.39	phalanx 1	*Ursus arctos taubachensis*	K V	22			
JN.5.40	phalanx 1	*Ursus arctos taubachensis*	K V	23			
JN.5.41	phalanx 1	*Ursus arctos taubachensis*	K V	20			
JN.5.42	phalanx 1	*Ursus arctos taubachensis*	K III	2			
JN.5.43	phalanx 1	*Ursus arctos taubachensis*	K III	17			
JN.5.44	phalanx 1	*Ursus arctos taubachensis*	K I	10			
JN.5.45	phalanx 2	*Ursus arctos taubachensis*	K V	23			
JN.5.46	phalanx 2	*Ursus arctos taubachensis*	K V	21			
JN.5.47	left c1	*Ursus arctos taubachensis*	K V	22			
JN.5.48	left c1	*Ursus arctos taubachensis*	K V	24			
JN.5.49	left C1	*Ursus arctos taubachensis*	K IV	16	K 2378		
JN.5.50	right p4	*Ursus arctos taubachensis*	K III	12			
JN.5.51	right p4	*Ursus arctos taubachensis*	K IV	18			
JN.5.52	left m1	*Ursus arctos arctos*	K II	21			
JN.5.53	left m1	*Ursus arctos arctos*	K V	24			
JN.5.54	crown of right m2	*Ursus arctos taubachensis*	K VI		K 35/87	0-15	1987
JN.5.55	right m3	*Ursus arctos taubachensis*	K V	23			
JN.5.56	left tibia	*Ursus arctos arctos*	K VI	7	K 678	660	
JN.5.57	left ulna	*Ursus arctos taubachensis*	K II	12			
JN.5.58	left humerus	*Ursus arctos taubachensis*	K VI	5		700	1992
JN.5.59	right humerus lack proximal epiphysis	*Ursus arctos taubachensis*	K III	6	K 594/77		
JN.5.60	right m1	*Ursus arctos taubachensis*	K II	22	K 2276		
JN.5.61	crown of right M2	*Ursus arctos taubachensis*	K VI		KH/3-90	135-150	1990
JN.5.62	crown of right M2	*Ursus arctos taubachensis*	K II	16			
JN.5.63	left m1	*Ursus arctos taubachensis*	K VI	3			
JN.5.64	left M2	*Ursus arctos taubachensis*	K II	23			
JN.5.65	left M2	*Ursus arctos taubachensis*	KCP			120-130	
JN.5.66	crown of left M2	*Ursus arctos taubachensis*	KCP			120-130	
JN.5.67	right m2	*Ursus arctos taubachensis*	K V	16			

JN.5.68	crown of right P3	*Ursus arctos taubachensis*	KCP			200-210	
JN.5.69	left p3	*Ursus arctos taubachensis*	KCP			200-210	
JN.5.70	crown of right p3	*Ursus arctos taubachensis*	KCP			130-140	
JN.5.71	left metacarpal 1	*Ursus arctos taubachensis*	KCP			220-230	1995
JN.5.72	left metacarpal 1	*Ursus arctos taubachensis*	K IV	16			
JN.5.73	right metacarpal 2	*Ursus arctos taubachensis*	K V	23	K-5-X		
JN.5.74	right metacarpal 2	*Ursus arctos taubachensis*	KCP			210-220	1994
JN.5.75	left metacarpal 2	*Ursus arctos taubachensis*	K V	23	K-5-X	50-60	1997
JN.5.76	right metacarpal 3	*Ursus arctos taubachensis*	KCP			80-90	1995
JN.5.77	right metacarpal 5	*Ursus arctos taubachensis*	K II	24			
JN.5.78	left metacarpal 5	*Ursus arctos taubachensis*	K III	21			
JN.5.79	left metatarsal 1	*Ursus arctos taubachensis*	KCP			100-110	1993
JN.5.80	right metatarsal 4	*Ursus arctos taubachensis*	K V	23			
JN.5.81	right calcaneus	*Ursus arctos taubachensis*	K IV	16			
JN.5.82	left metacarpal 4	*Ursus arctos taubachensis*	K V	23	K-5-X		
JN.5.83	right metatarsal 4	*Ursus arctos taubachensis*	KCP			20-30	1997
JN.5.84	right ulna	*Ursus arctos taubachensis*	K II	22			
JN.5.85	left tibia	*Ursus arctos taubachensis*	KCP			200-210	1996
JN.5.86	right tibia	*Ursus arctos taubachensis*	K I	14			
JN.5.87	left humerus without proximal epiphysis	*Ursus arctos arctos*	K III	19			
JN.5.88	distal epiphysis of right humerus	*Ursus arctos taubachensis*	K II	22			
JN.5.89	left humerus without proximal epiphysis	*Ursus arctos taubachensis*	K IV	13			
JN.5.90	right P4	*Ursus arctos taubachensis*	K III	22			
JN.5.91	right P4	*Ursus arctos taubachensis*	K II	11			
JN.5.92	right P4	*Ursus arctos taubachensis*	K VI			10-20	1991
JN.5.93	slightly worn crown of left M1	*Ursus arctos taubachensis*	K IV	23			
JN.5.94	left M1	*Ursus arctos taubachensis*	K V	25			
JN.5.95	right M1	*Ursus arctos taubachensis*	K II	15			
JN.5.96	crown of right M1	*Ursus arctos taubachensis*	K VI			10-20	1991
JN.5.97	crown of left M2	*Ursus arctos taubachensis*	K I	1			
JN.5.98	right M2	*Ursus arctos taubachensis*	K III	3			
JN.5.99	slightly worn crown of left M2	*Ursus arctos taubachensis*	K IV	4			
JN.5.100	right mandible with c1-p1 and p4-m3	*Ursus arctos arctos*	K VI			0-10	1990
JN.5.101	crown of right m1	*Ursus arctos taubachensis*	K II	26			
JN.5.102	left m1	*Ursus arctos taubachensis*	K III	5			
JN.5.103	left m2	*Ursus arctos taubachensis*	K II	11			
JN.5.104	right m3	*Ursus arctos arctos*	K IV	4			
JN.5.105	left calcaneus	*Ursus arctos arctos*	K II	23			
JN.5.106	right calcaneus	*Ursus arctos taubachensis*	K III	4			
JN.5.107	right metatarsal 4	*Ursus arctos taubachensis*	K VI			135-150	1991
JN.5.108	right metacarpal 4	*Ursus arctos taubachensis*	K V	23	K-5-X		

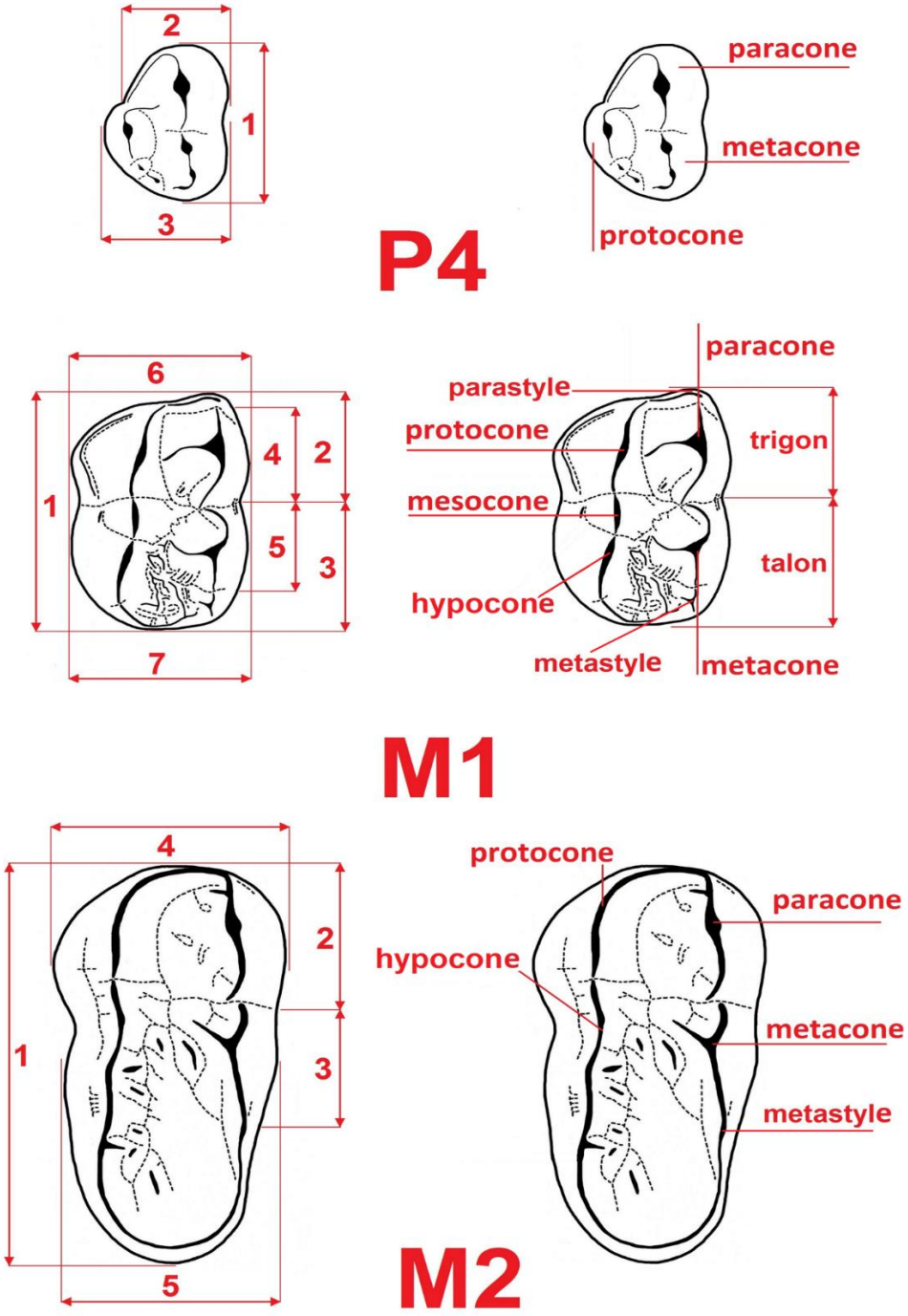

APPENDIX 2

Figure S1. Scheme of measurements and cusps terminology of the ursid upper cheek teeth.

P4:

1 - total length (L),
2 - trigon breadth (B tr),
3 - talon breadth (B ta).

M1:

1 - total length (L),
2 - trigon length (L tr),
3 - talon length (L ta),
4 - paracone length (L pa),
5 - metacone length (L me),
6 - trigon breadth (B tr),
7 - talon breadth (B ta).

M2:

1 - total length (L),
2 - paracone length (L pa),
3 - metacone length (L me),
4 - trigon breadth (B tr),
5 - talon breadth (B ta).

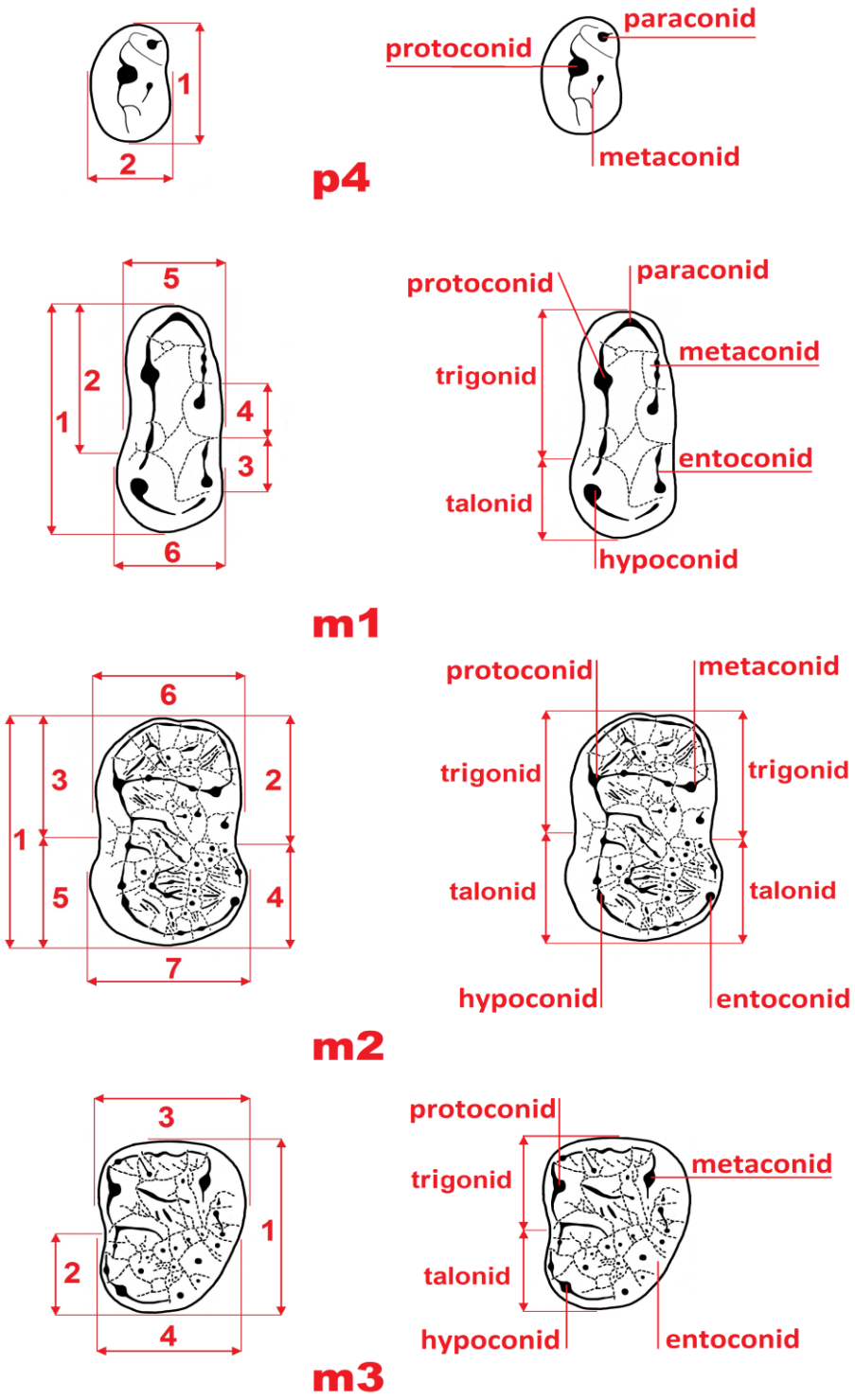

Figure S2. Scheme of measurements and cusps terminology of the ursid lower cheek teeth.

p4:
1 - total length (L),
2 - total breadth (B).

m1:
1 - total length (L),
2 - trigonid length (L tr),
3 - length of distal entoconid (L e1),
4 - length of mesial entoconid (L e2),
5 - trigonid breadth (B tr),
6 - talonid breadth (B ta).

m2:
1 - total length (L),
2 - trigonid lingual length (L tr 1),
3 - trigonid buccal length (L tr 2),
4 - talonid lingual length (L ta 1),
5 - talonid buccal length (L ta 2),
6 - trigonid breadth (B tr),
7 - talonid breadth (B ta).

m3:
1 - total length (L),
2 - talonid length (L la),
3 - trigonid breadth (B tr),
4 - talonid breadth (B ta).

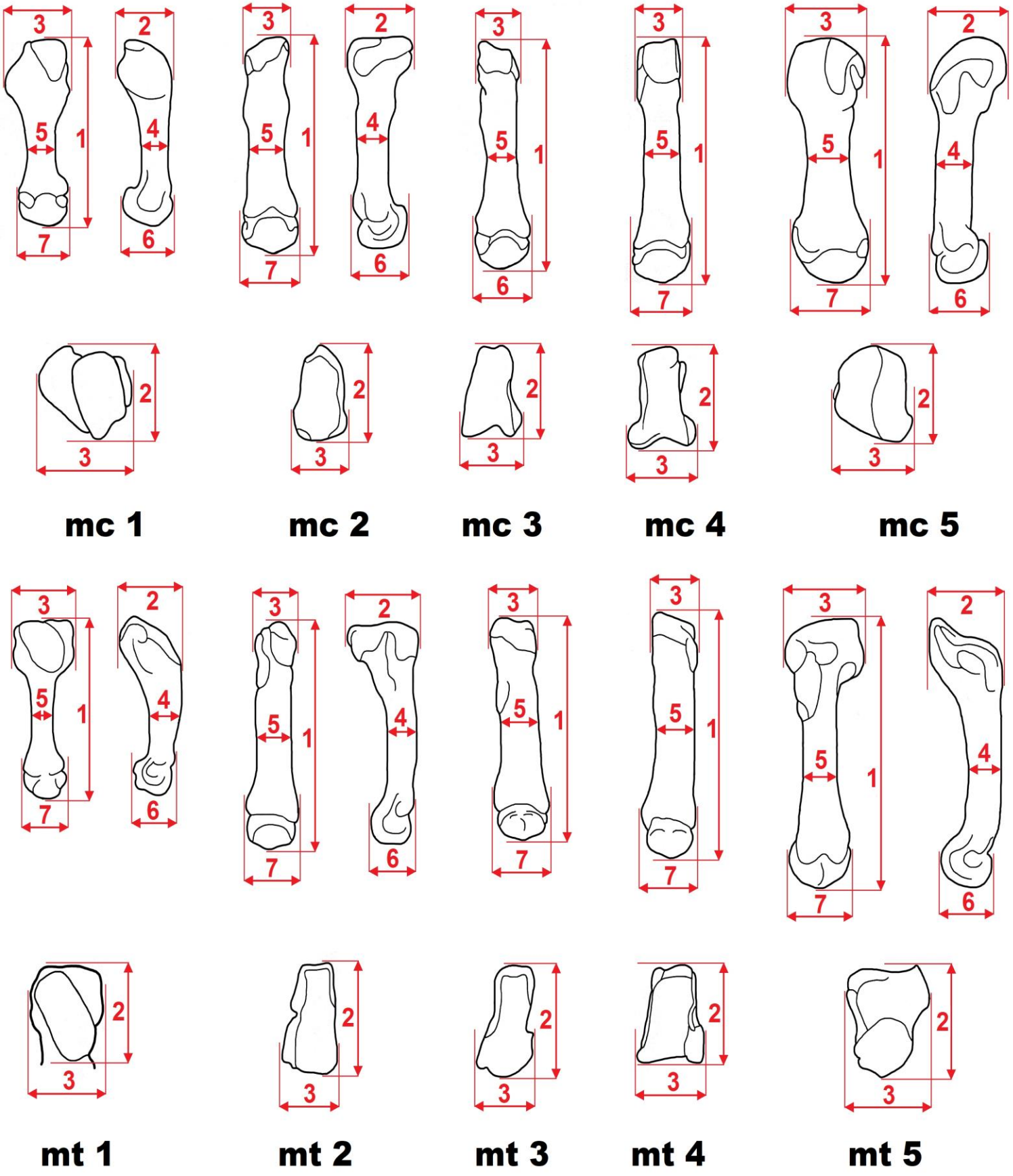

Figure S3. Scheme of measurements of ursid metacarpals and metatarsals:
1 - total length (L),
2 - proximal epiphysis depth (pL),
3 - proximal epiphysis breadth (pB),
4 - shaft depth (mL),
5 - shaft breadth (mB),
6 - distal epiphysis depth (dL),
7 - distal epiphysis breadth (dB).

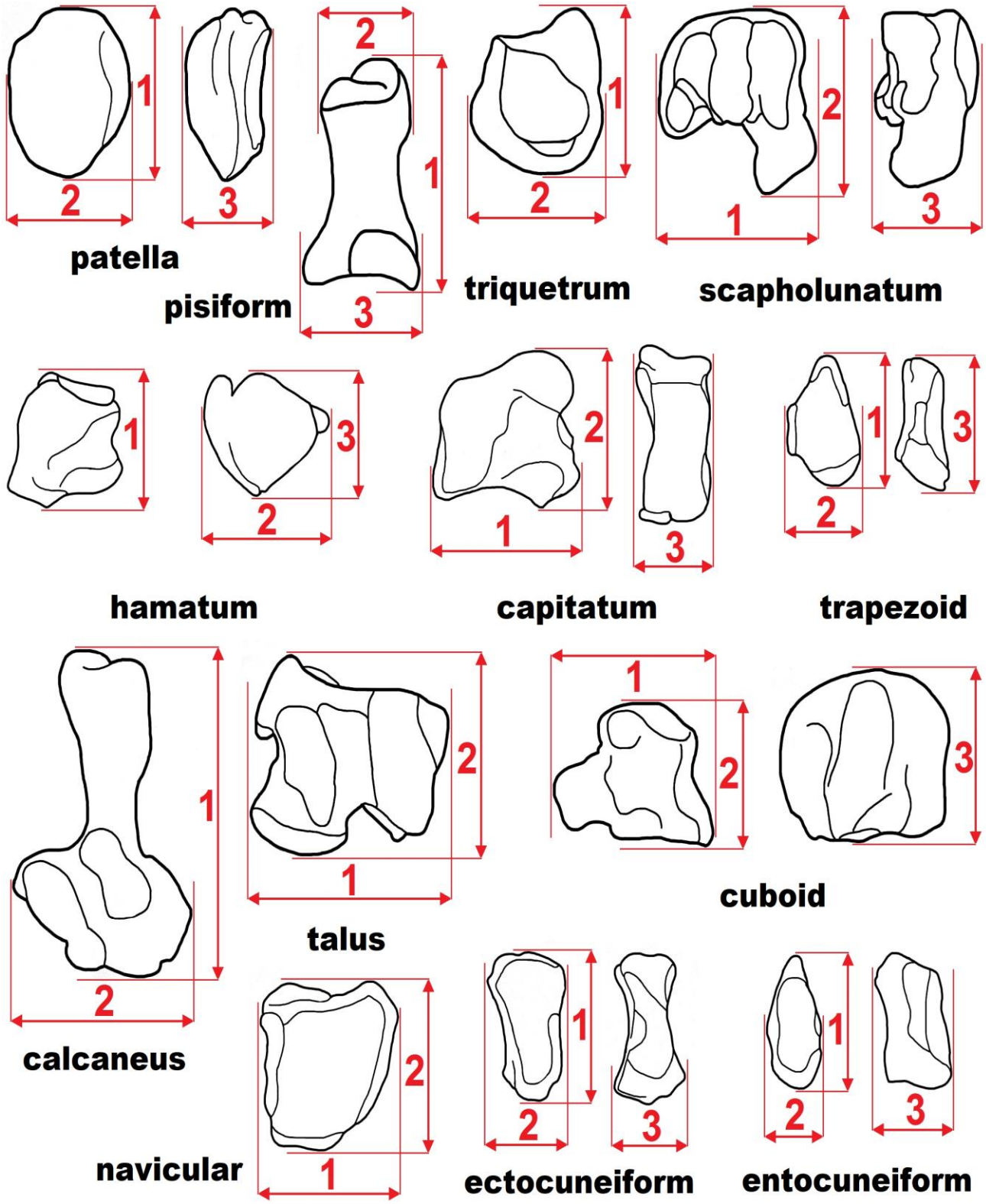

Figure S4. Scheme of measurements of ursid carpals and tarsals:

1 - length (L),

2 - breadth (B),

3 - depth (D).